Submitted to Physical Review D

FERMILAB–Pub–95/406-A
CERN-TH/96-112
E-Print astro-ph/9612222

# A Fresh Look at Axions and SN 1987A

Wolfgang Keil and Hans-Thomas Janka

*Max-Planck-Institut für Astrophysik*

*Karl-Schwarzschild-Str. 1, 85740 Garching, Germany*

David N. Schramm, Günter Sigl, and Michael S. Turner

*Department of Astronomy & Astrophysics*

*Enrico Fermi Institute, The University of Chicago, Chicago, IL 60637-1433*

*NASA/Fermilab Astrophysics Center*

*Fermi National Accelerator Laboratory, Batavia, IL 60510-0500*

John Ellis

*Theoretical Physics Division, CERN, CH-1211 Geneva 23, Switzerland*



## Abstract

We re-examine the very stringent limits on the axion mass based on the strength and duration of the neutrino signal from SN 1987A, in the light of new measurements of the axial-vector coupling strength of nucleons, possible suppression of axion emission due to many-body effects, and additional emission processes involving pions. The suppression of axion emission due to nucleon spin fluctuations induced by many-body effects degrades previous limits by a factor of about 2. Emission processes involving thermal pions can strengthen the limits by a factor of 3–4 within a perturbative treatment that neglects saturation of nucleon spin fluctuations. Inclusion of saturation effects, however, tends to make the limits less dependent on pion abundances. The resulting axion mass limit also depends on the precise couplings of the axion and ranges from $0.5 \times 10^{-3}$ eV to $6 \times 10^{-3}$ eV.

PACS numbers: 14.80.Mz, 97.60.Bw, 21.65.+f, 95.30.Cq

## I. INTRODUCTION

Peccei-Quinn (PQ) symmetry [1] continues to be an attractive solution to the strong $CP$ problem. However, theory and laboratory experiment give little guidance on the PQ symmetry-breaking scale, $f_a$, and therefore on the mass of the pseudo-Goldstone boson associated with PQ symmetry, the axion [2]:

$$m_a \simeq 0.62\,\mathrm{eV} \cdot 10^7\,\mathrm{GeV}/f_a \ . \tag{1}$$

Astrophysical and cosmological arguments have been very powerful in excluding values of the axion mass, allowing only the mass range from about $10^{-6}\,\mathrm{eV}$ to about $10^{-3}\,\mathrm{eV}$ [3].

Axions in this mass range would have been produced cosmologically by a coherent, non-thermal mechanism [4]. Because of this, axions in this mass range would be cosmologically significant, have small velocities, and behave as cold dark matter (CDM), in spite of their small mass. Depending upon cosmological and particle physics parameters, axions could contribute to the closure mass density today for $m_a \simeq 10^{-6}\,\mathrm{eV}$ to $10^{-4}\,\mathrm{eV}$ [5]. We recall also that the CDM scenario for structure formation is at present the most promising [6], with axions and neutralinos being the leading CDM candidates. If axions provide the bulk of the dark matter, they must comprise a significant fraction of the dark halo of our own galaxy [7], and a large-scale experiment is underway to detect halo axions of mass $10^{-6}\,\mathrm{eV}$ to $10^{-5}\,\mathrm{eV}$ [8].

The most stringent astrophysical bound on the axion mass is that derived from observations of neutrinos from SN 1987A, excluding masses greater than about $10^{-3}\,\mathrm{eV}$ [9,10]. It is based upon the detection of 19 neutrinos from SN 1987A by the Kamiokande II (KII) [11] and Irvine-Michigan-Brookhaven (IMB) [12] water-Cherenkov detectors. According to the standard model of Type II supernovae, namely the core collapse of a massive star, these neutrinos were emitted during the early cooling phase of the nascent neutron star associated with the appearance of SN 1987A. Indeed, the observed neutrino flux and energy spectrum are consistent with this picture [13]. The emission of axions would have hastened the cooling process, leading to fewer events over a shorter time. The axion's couplings to ordinary matter are proportional to the axion mass, so consistency with the detected neutrino burst leads to an upper limit to the axion mass, which is estimated to be around $10^{-3}\,\mathrm{eV}$.

A number of questions have been raised about the mass limit based upon SN 1987A. They include the possible suppression of axion emission by many-body effects which are likely to be important in the deep interior of a neutron star [14–16], enhancement of axion emission due to the possible presence of kaons and thermal pions at the centers of neutron stars [17], and the implications of recent measurements of the strengths of axial-current couplings to nucleons, which may lead to a significant suppression of the axion-neutron coupling relative to estimates based on the naive quark model (NQM) [16].

The purpose of this paper is to address these issues; its outline is as follows. Sect. II is devoted to a discussion of the axion-nucleon couplings and a description of the input microphysics of the numerical protoneutron star models. The axion emission rates are reviewed in Sect. III, including many-body effects, with particular attention to the possible damping effects of nucleon spin fluctuations. Sect. IV discusses cooling models and the impact of axion emission on the theoretical predictions for the neutrino bursts detected by KII and IMB. We finish with a summary of our results in Sect. V.

## II. INPUT PHYSICS

### A. Axion Couplings

The most important axion-emission process in a hot, young neutron star is axion bremsstrahlung when two nucleons collide. The rate for this process depends upon the axion's coupling to nucleons. The relevant part of the interaction Lagrangian is

$$\mathcal{L}_{\rm int} = \frac{g_{ai}}{2m_i}\bar{\psi}_i\gamma_\mu\gamma_5\psi_i\,\partial^\mu a\ , \tag{2}$$

where the index $i$ denotes a neutron or proton, and we can write the axion-nucleon couplings $g_{ai}$ in the form

$$g_{ai} \equiv C_i m_i/(f_{\rm PQ}/N) \equiv C_i m_i/f_a\ . \tag{3}$$

$N$ is the color anomaly of the PQ symmetry. The dimensionless couplings $C_i$ of Eq. (3) are of order unity, and related by generalized Goldberger-Treiman relations to nucleon axial-vector current matrix elements via the PQ charges $x_q$ of the light quarks $q = u, d, s$:

$$\begin{aligned} C_p &= [x_u - 1/(1+z+w)]\Delta u + [x_d - z/(1+z+w)]\Delta d + [x_s - w/(1+z+w)]\Delta s; \\ C_n &= [x_u - 1/(1+z+w)]\Delta d + [x_d - z/(1+z+w)]\Delta u + [x_s - w/(1+z+w)]\Delta s; \end{aligned} \tag{4}$$

where we use for the light-quark mass ratios

$$z \equiv m_u/m_d \simeq 0.565\,,\ \ w \equiv m_u/m_s \simeq 0.029\ . \tag{5}$$

The PQ charges of the quarks are model dependent: they vanish for the KVSZ axion [18], $x_u = x_d = x_s = 0$, whilst for the DFSZ axion [19] they can be written in terms of an angle $\beta$ which is related to a ratio of Higgs vacuum expectation values:

$$x_u = \sin^2\beta/3,\ x_d = x_s = \cos^2\beta/3 \tag{6}$$

The $\Delta q$ in Eq. (4) quantify the axial-vector current couplings to the proton:

$$\Delta q\, S_\mu \equiv \langle p|\bar{q}\gamma_\mu\gamma_5 q|p\rangle \tag{7}$$

where $S_\mu$ is the proton spin. Similar expressions hold for the neutron, with matrix elements related by an isospin reflection: $\Delta u_n = \Delta d, \Delta d_n = \Delta u$.

The $\Delta q$ are non-perturbative quantities whose values must be taken from experiment. Neutron $\beta$ decay and isospin invariance constrain $\Delta u - \Delta d \equiv g_A \simeq 1.25$, whilst hyperon $\beta$ decays and flavor $SU(3)$ symmetry for the baryon octet yield $\Delta u + \Delta d - 2\Delta s \simeq 0.682$. The best determinations of the third combination of the $\Delta q$ are obtained from spin-dependent deep-inelastic electron and muon scattering off nucleons. Recent analyses give [20]:

$$\begin{aligned} \Delta u &= \ \ 0.80 \pm 0.04 \pm 0.04\,; \\ \Delta d &= -0.46 \pm 0.04 \pm 0.04\,; \\ \Delta s &= -0.12 \pm 0.04 \pm 0.04\,; \end{aligned} \tag{8}$$

where the first error is a statistical error, and the second is an estimated systematic error. The values in Eq. (8) are quite different from those estimated in the NQM, which does not estimate axial-current matrix elements reliably. As can be seen in Eq. (4), the measurements of Eq. (8) and the PQ charges of the light quarks determine the axion-nucleon couplings. Values for the KSVZ and DFSZ axions are shown in Fig. 1.

It is perhaps worth warning the reader at this point that the above values of the $\Delta q$ have been obtained for nucleons that are free, or in light nuclei. It is possible that the axial-vector current couplings may be different for nucleons in a dense medium. However, large effects on these couplings are not seen in conventional nuclear physics, and we believe that other many-body effects on the axion emission rate are dominant, as we discuss in Sect. III C.

### B. Protoneutron Star Physics

In order to obtain limits on the axion production in SN 1987A and thus on the axion mass, we performed numerical simulations of the evolution of newly formed neutron stars. The simulations started a few milliseconds after core bounce and supernova shock formation and followed the Kelvin-Helmholtz cooling by neutrino emission until the lepton-rich and hot protoneutron star had evolved to the final cold and neutronized state several ten seconds later. Cooling sequences were computed with and without axion emission included, and the corresponding neutrino luminosities and spectra were used to derive predictions for the associated KII and IMB detector signals.

The initial models of the protoneutron star were constructed with profiles of the electron concentration $Y_e = n_e/n_b$ ($n_e$ is the electron number density, $n_b$ the baryon number density) and of the temperature $T$ that were very close to those obtained in detailed hydrodynamical calculations of stellar core collapse [21]. The collapsed stellar core right after core bounce is gravitationally only weakly bound. This is expressed by the fact that the ratio of the gravitational mass at the beginning of the simulation, $M^{\rm i}_{\rm ns,g}$, to the baryonic mass, $M_{\rm ns,b}$, is only slightly less than unity. We scaled the temperature profiles from given numerical models of post-collapse cores such that $M^{\rm i}_{\rm ns,g}/M_{\rm ns,b} = 0.97$ in all of our initial setups. The baryonic mass of the neutron star depends on the mass of the progenitor star of the supernova. Simulations with varied protoneutron star mass [22,25] showed that the neutrino signal from SN 1987A can be best reproduced by models with a mass of $M_{\rm ns,b} \simeq 1.5 \ldots 1.6\, M_\odot$. The reference model of the simulations presented here was therefore chosen to have $M_{\rm ns,b} = 1.53\, M_\odot$ and an initial gravitational mass of $M^{\rm i}_{\rm ns,g} = 1.49\, M_\odot$. The electron number fraction had a maximum at the center of the star where $Y^{\rm i}_{e,{\rm c}} \simeq 0.29$. The central temperature and density at the beginning of the simulations were $T^{\rm i}_{\rm c} = 24\,{\rm MeV}$ and $\rho^{\rm i}_{\rm c} = m \times 0.485\,{\rm fm}^{-3} \cong 8 \times 10^{14}\,{\rm g\,cm}^{-3} \simeq 3.25\rho_{\rm nuc}$, respectively, with $\rho_{\rm nuc}$ being the nuclear matter density and $m$ the common nucleon mass.

The computations were done with a general relativistic stellar evolution code [22] employing equations of state developed for the case $T = 0$ by Glendenning [23] and extended to finite temperatures by including thermal corrections to the energy density and pressure of both stellar plasma and neutrinos [22]. Two different equations of state were employed. As the standard case, we used a hyperon equation of state (case 2 in [23]; EOS B in [22]) which takes into account $n$, $p$, $e^\pm$, and $\mu^-$ in the nuclear medium, and hyperons ($\Lambda$, $\Sigma$ ...) and $\Delta$-resonances as additional hadronic states at densities above about $2\rho_{\rm nuc}$. Due to the

formation of these additional baryonic degrees of freedom, the hyperon equation of state is "softer" at very high densities than a non-hyperonic equation of state involving only $n$, $p$, $e^{\pm}$ and $\mu^{-}$. An equation of state of the latter category (case 5 in [23], EOS A in [22]) was used for comparative computations in the work presented here.

The equations of state employed here do not predict the occurrence of pions or pion condensates in the supernova core. The possible importance of pionic excitations was pointed out in a paper by Mayle, Tavani, and Wilson [24]. The presence of a significant number of negative thermal pions influences the axion emission from forming neutron stars by producing axions via pion-axion conversion processes $\pi^{-}+p \rightarrow n+a$ (Sect. III B and [17]). In order to estimate the impact of the latter on the protoneutron star cooling, we computed a number of models using the rather crude assumption that one $\pi^{-}$ per nucleon is present at densities beyond about two times nuclear matter density. The local abundance $Y_{\pi^-} = n_{\pi^-}/n_{\rm b}$ was simply prescribed by $Y_{\pi^-} = Y_N \cdot \{1+\tanh[2(\rho-\rho_{\rm nuc})/\rho_{\rm nuc}]\}/2$ with $\rho_{\rm nuc} = m \times 0.15\,{\rm fm}^{-3}$. This prescription is ad hoc and effects of pions on the nuclear equation of state were not taken into account at all. Also, we ignored the temperature dependence of the abundance of thermal pions. Our choice of $Y_{\pi^-}$ of order unity was motivated by the results of Ref. [24], where an abundance of $Y_{\pi^-} \lesssim 0.6$ (and a total pion abundance of $Y_{\pi} \lesssim 0.8$) was obtained for the conditions of temperature and density in a neutron star model at 3 s after core bounce. The possibility of a pion condensate, however, was excluded for the supernova conditions and the pion dispersion relation assumed in Ref. [24]. Since our whole treatment of the pion case was very approximate only, we also did not make any attempt to include the contributions of pions to the neutrino scattering opacity of the nuclear medium (see also [24]).

As for the neutrino transport, equilibrium diffusion was assumed for all types of neutrinos ($\nu_e$, $\bar{\nu}_e$, $\nu_\mu$, $\bar{\nu}_\mu$, $\nu_\tau$, $\bar{\nu}_\tau$) which is a good approximation, because the hot matter of the protoneutron star is very opaque against neutrinos by neutral-current neutrino-nucleon scatterings, $\nu+N \rightarrow \nu+N$, and charged-current $\beta$-reactions, $\nu_e+n \rightarrow e^{-}+p$ and $\bar{\nu}_e+p \rightarrow e^{+}+n$. For details of the technical implementation and the "standard" description of neutrino-matter interactions, see [22]. A possible reduction of the neutrino opacity by many-body correlation effects, e.g., a suppression of the $\nu N$ scattering cross section by rapid spin fluctuations due to frequent nucleon-nucleon collisions ( [14–16,25,26] and Sect. III C), was included only in a comparative model run to reveal the change of the axion mass limit. We want to emphasize here that the central density of our reference neutron star model with $M_{\rm ns,b} = 1.53\,M_\odot$ is always less than $8.8 \times 10^{14}\,{\rm g\,cm^{-3}}$. Only in a relatively small, central part with a mass $\lesssim 0.5\,M_\odot$ does the density become higher than about $2\rho_{\rm nuc}$ and hyperonization sets in. But even at the center of the star the hyperon abundance $Y_{\rm hyp} = n_{\rm hyp}/n_{\rm b}$ never rises above $Y_{\rm hyp} \simeq 0.25$ (see Fig. 7 in [23]). Therefore we consider the disregard of modifications of the neutrino opacity due to the presence of hyperons [27] as acceptable for the models discussed in this work, and the assumption that the neutrino opacity is produced mainly by interactions of neutrinos with $n$ and $p$ should yield a sufficiently accurate description.

In order to evaluate our protoneutron star cooling models for the prediced neutrino signals in the KII and IMB detectors, we folded the computed spectral $\bar{\nu}_e$ number flux with the detector efficiency functions and the cross section for $\bar{\nu}_e$ absorption on protons. A distance to SN 1987A of $D = 50\,{\rm kpc}$ was assumed. For details of the evaluation procedure, see Appendix C of [22].

## III. AXION EMISSION RATES

### A. Nucleon-Nucleon Axion Bremsstrahlung

As long as the widths of the nucleon states are small compared to the temperature, one can evaluate the matrix elements for nucleon-pair bremsstrahlung of axions by using free nucleon states. A one-pion exchange (OPE) potential is likely to be an adequate starting-point for describing the two-nucleon interaction. As a function of the four-momentum transfer between the nucleons, $k = (k_0, \mathbf{k})$, it can be written as [28]

$$V_{\rm OPE}(\mathbf{k}, \boldsymbol{\sigma}_1, \boldsymbol{\sigma}_2) = -\left(\frac{f}{m_\pi}\right)^2 \frac{(\boldsymbol{\sigma}_1 \cdot \mathbf{k})\,(\boldsymbol{\sigma}_2 \cdot \mathbf{k})}{k^2 + m_\pi^2}\,(\boldsymbol{\tau}_1 \cdot \boldsymbol{\tau}_2)\ . \tag{9}$$

Here, $f \simeq 1$ is the pion-nucleon coupling constant, $m_\pi$ is the pion mass, and $\boldsymbol{\sigma}_j$ and $\boldsymbol{\tau}_j$ are spin and isospin operators for the two nucleons, respectively ($j = 1, 2$). The resulting matrix element $\mathcal{M}$ was first calculated in Ref. [29] for degenerate nucleons and later in [30] for arbitrary nucleon degeneracy. The lowest-order energy-loss rate per unit volume due to axion emission, $Q_a^{(1)}$, is then given by the phase-space integral

$$\begin{aligned} Q_a^{(1)} = \int \frac{d^3\mathbf{k}_a}{2\omega(2\pi)^3} \prod_{j=1}^{4} \frac{d^3\mathbf{p}_j}{2E_j(2\pi)^3}\, \omega f_1 f_2 (1-f_3)(1-f_4) \\ \times S \sum_{\rm spins} |\mathcal{M}|^2 (2\pi)^4 \delta^4(p_1 + p_2 - p_3 - p_4 - k_a)\,, \end{aligned} \tag{10}$$

where $p_j = (E_j, \mathbf{p}_j)$ are the four-momenta of the initial-state ($j = 1, 2$) and final-state ($j = 3, 4$) nucleons, and $k_a = (\omega, \mathbf{k}_a)$ is the axion four-momentum. Furthermore, $f_j$ is the nucleon occupation number in state $p_j$ ($j = 1, \cdots, 4$), and $S$ is the usual symmetry factor.

In Ref. [30] the 15-dimensional integration in Eq. (10) was performed exploiting the fact that $|\mathcal{M}|^2$ varies only slightly in the range where the integrand contributes most. Neglecting this variation induces an error of less than a factor 2. Introducing the thermal average

$$\xi \equiv 3 \left\langle \left[ \frac{(\mathbf{p}_2 - \mathbf{p}_4) \cdot (\mathbf{p}_2 - \mathbf{p}_3)}{|\mathbf{p}_2 - \mathbf{p}_4||\mathbf{p}_2 - \mathbf{p}_3|} \right]^2 \right\rangle \tag{11}$$

which can be shown to take the values 0 and 1.0845 in the limits of degenerate and non-degenerate nucleons, respectively, the result can be written as

$$\begin{aligned} Q_a^{(1)} = 64 \left(\frac{f}{m_\pi}\right)^4 m^{2.5} T^{6.5} \Bigg[ & (1-\xi/3) g_{an}^2 I(y_n, y_n) + (1-\xi/3) g_{ap}^2 I(y_p, y_p) \\ & + \frac{4(15-2\xi)}{9} \left(\frac{g_{an}^2 + g_{ap}^2}{2}\right) I(y_n, y_p) + \frac{4(6-4\xi)}{9} \left(\frac{g_{an} + g_{ap}}{2}\right)^2 I(y_n, y_p) \Bigg]. \end{aligned} \tag{12}$$

Here, $y_i$ is the dimensionless non-relativistic version of the nucleon chemical potential $\mu_i$: $y_i = (\mu_i - m_i)/T$, and the dimensionless function $I(y_1, y_2)$ can be fitted to within 25% accuracy by the analytic expression [30]

$$I(y_1,y_2) \simeq \Big[2.39\times10^5\left(e^{-y_1-y_2}+0.25e^{-y_1}+0.25e^{-y_2}\right)+1.73\times10^4(1+|\bar{y}|)^{-1/2}$$
$$+6.92\times10^4(1+|\bar{y}|)^{-3/2}+1.73\times10^4(1+|\bar{y}|)^{-5/2}\Big]^{-1}\,, \tag{13}$$

with $\bar{y}=(y_1+y_2)/2$.

### B. Pion-Axion Conversion

If pions or kaons are present in a supernova core, additional processes such as $\pi^-+p\to n+a$ can contribute to axion emission. Since it is uncertain whether a pion condensate can form in the hot protoneutron star [24], we consider only thermal pions here. The corresponding lowest-order perturbative energy emission rate per unit volume was found to be [17]

$$Q_a^{\pi^-}=\frac{30f^2\bar{g}_{aN}^2T^3}{\pi m^2 m_\pi^2}\,n_{\pi^-}n_p\,, \tag{14}$$

where $\bar{g}_{aN}$ is a combination of axion-proton and axion-neutron couplings,

$$\bar{g}_{aN}^2=\frac{1}{2}\left(g_{ap}^2+g_{an}^2\right)-\frac{1}{3}\,g_{ap}g_{an}\,, \tag{15}$$

and $n_{\pi^-}$ and $n_p$ are the number densities of $\pi^-$ and protons. If the pion abundance is comparable to the nucleon abundance, energy loss by pion-axion conversion will dominate over nucleon-pair bremsstrahlung of axions by more than a factor of 10 [17] in the perturbative approximation, i.e., when saturation due to many-body effects in the dense medium (see Sect. III C) are ignored. We have considered the axion mass bounds resulting from the lowest-order pion-axion emission rate as well. Due to the clear dominance of the axion emission from pion conversion processes in the perturbative approximation, we neglected the production of axions by nucleon-nucleon bremsstrahlung when $\pi^-$ were assumed to be present in the cooling neutron star.

### C. Many-Body Effects

Recently the possibility was discussed [14–16,26] that near nuclear densities many-body effects might suppress substantially the actual energy-loss rate in axions compared to the lowest-order result Eq. (12). A suppression is likely to occur also for the rate of Eq. (14). In order to discuss this issue and to compare different approaches, it is convenient to reformulate the loss rate in terms of the structure function formalism adopted in these references. In the limit of non-relativistic nucleons, axions couple exclusively to the dynamical spin-density structure function (SSF), as can be seen from Eq. (2). Its long-wavelength limit is defined as

$$S_\sigma(\omega)=\lim_{\mathbf{k}\to0}\frac{4}{3n_b}\int_{-\infty}^{+\infty}dt e^{i\omega t}\left\langle\boldsymbol{\sigma}(t,\mathbf{k})\cdot\boldsymbol{\sigma}(0,-\mathbf{k})\right\rangle\,. \tag{16}$$

Here, $\boldsymbol{\sigma}(t,\mathbf{k}) = V^{-1}\int d^3\mathbf{r} e^{-i\mathbf{k}\cdot\mathbf{r}}\boldsymbol{\sigma}(t,\mathbf{r})$ (with $V$ the normalization volume) is the Fourier transform of the local nucleon spin-density operator $\boldsymbol{\sigma}(t,\mathbf{r})$, $n_b$ is the baryon density, and $(\omega,\mathbf{k})$ is the four-momentum transfer to the medium. The expectation value $\langle\cdots\rangle$ in Eq. (16) is taken over a thermal ensemble and the states involved are normalized to $V$. For a single species of nucleons whose coupling to axions is given by $C_i$ [see Eqs. (2)–(4)] $Q_a$ can then be written as [16,26]

$$Q_a = \frac{C_i^2 n_b}{(4\pi)^2 f_a^2}\int_0^\infty d\omega\,\omega^4 e^{-\omega/T} S_\sigma(\omega)\,. \tag{17}$$

For two nucleon species one can absorb the constant $C_i^2$ into the definition of $S_\sigma$ by multiplying $\boldsymbol{\sigma}(t,\mathbf{k})$ in Eq. (16) by $[1+\tau_3(t,\mathbf{k})]\,C_p/2 + [1-\tau_3(t,\mathbf{k})]\,C_n/2$. Here, $\tau_3(t,\mathbf{k})$ is the third component of the isospin operator $\boldsymbol{\tau}(t,\mathbf{k})$ which is defined analogously to $\boldsymbol{\sigma}(t,\mathbf{k})$. For the qualitative discussion in the rest of this section, it is sufficient to focus on the case of a single nucleon species if not stated otherwise.

It is obvious from Eq. (16) that only interactions which do not conserve the total nucleon spin can lead to non-vanishing values of $S_\sigma(\omega)$ at $\omega \neq 0$. As can be seen easily, the OPE potential Eq. (9) has this property. For the following, it is convenient to introduce the lowest-order effective spin fluctuation rate,

$$\Gamma_\sigma^{(1)} \equiv \frac{1}{3\pi}\left(\frac{f}{m_\pi}\right)^4 m^2 n_b \langle v\rangle \simeq 32\,\mathrm{MeV}\rho_{14}T_{10}^{1/2}\,, \tag{18}$$

where $\langle v\rangle$ is the average relative velocity between two nucleons, $\rho_{14}$ is the mass density in units of $10^{14}\mathrm{gcm}^{-3}$, and $T_{10} = T/10\,\mathrm{MeV}$. In the limit of non-degenerate nucleons, the lowest-order contribution to the SSF takes the form [15]

$$S_\sigma^{(1)}(\omega) = \frac{K\Gamma_\sigma^{(1)}}{\omega^2}\,s_0(\omega/T)\,, \tag{19}$$

where $K = 12\pi^{-1/2}\,(T/m)^{1/2}\,/\,\langle v\rangle \simeq 2.7$ [1]. The dimensionless bounded function $s_0(\omega/T)$ has been given in Ref. [15]. Adopting Eq. (19) in Eq. (17) leads to a rate $Q_a$ which, for the case of two nucleon species, coincides with Eq. (12) in the non-degenerate limit, $y_n, y_p \ll -1$. Note that, according to Eq. (13), $I(y_1,y_2)\propto e^{y_1+y_2}\propto n_1 n_2 T^{-3}$ in this limit, where $n_i$ is the number density of species $i$.

However, Eq. (19) is unphysical in the limit of both small and large energy transfers, which can be seen as follows. First, one can derive the sum rule,

$$\int_{-\infty}^{+\infty}\frac{d\omega}{2\pi}\,S_\sigma(\omega) = 1 + \frac{4}{3n_bV}\left\langle\sum_{i\neq j}\boldsymbol{\sigma}_i\cdot\boldsymbol{\sigma}_j\right\rangle\,, \tag{20}$$

where the sum over all nucleon pairs accounts for possible spin correlations among different nucleons. At least at low densities, these correlations can be neglected compared to the first

---

[1] The relation between our $\Gamma_\sigma^{(1)}$ defined in Eq. (18) and the quantity $\Gamma_A$ used in Ref. [15] is $\Gamma_A = K\Gamma_\sigma^{(1)}$.

term. In any case, the finiteness of the integral in Eq. (20) clearly shows that the infrared singularity in Eq. (19) is unphysical. In fact, higher-order effects are expected to regularize this singularity at low energy transfers. As a first qualitative guess, it was suggested [15] to substitute $\omega^{-2}$ by $(\omega^2 + a^2\Gamma_\sigma^2)^{-1}$, where $a$ is a dimensionless number of order unity which can be chosen to satisfy the sum rule Eq. (20).

Secondly, one of us (G.S.) [26] recently derived the analog of what is usually called the f sum rule,

$$\int_{-\infty}^{+\infty} \frac{d\omega}{2\pi}\, \omega S_\sigma(\omega) = -\frac{4}{n_b V}\langle H_T\rangle \equiv \frac{2\Gamma_\sigma}{\pi}\,, \tag{21}$$

where $H_T = \frac{1}{2}\sum_{i\neq j} V_{ij}^T$ is the "tensor component" of the nucleon interaction Hamiltonian, defined as the tensor component $V_{ij}^T$ of the two-nucleon interaction potential [31], summed over all pairs. It is this component which violates local nucleon spin conservation and, according to Eq. (21), determines the width of the SSF via the effective spin fluctuation rate

$$\Gamma_\sigma \equiv \frac{-2\pi\,\langle H_T\rangle}{n_b V}\ . \tag{22}$$

$\Gamma_\sigma^{(1)}$ defined in Eq. (18) can be shown to be the first-order approximation to $\Gamma_\sigma$ in a dilute medium. It turns out that in the case of two nucleon species the f sum, Eq. (21), diverges when Eq. (19) is substituted for the SSF [26]. This can be traced back to the unphysical behavior of the dipole-like OPE potential Eq. (9) at small distances. More realistic potentials which account for hard-core repulsion lead to a fall off of $S_\sigma$ at high $\omega$ which is stronger than $\omega^{-2}$, thus assuring f sum integrability.

A plausible modification of the SSF is given by

$$S_\sigma(\omega) = \frac{K\Gamma_\sigma}{\omega^2 + a^2\Gamma_\sigma^2}\, s(\omega/T)\,, \tag{23}$$

where the continuous and bounded function $s(\omega/T)$ is even and satisfies $s(0) = 1$. This expression has the right limiting behavior in the classical regime which obtains for $\omega \ll T$ [32]. For $\omega \lesssim \Gamma_\sigma$, multiple collisions become important and lead to a suppression of $S_\sigma(\omega)$ compared to the lowest-order approximation Eq. (19), which is known as the Landau-Pomeranchuk-Migdal effect [33,34] and ensures integrability of the sum rule Eq. (20). In the classical bremsstrahlung limit of hard collisions one would have $s(x \equiv \omega/T) \equiv 1$. Quantum corrections require that $s(x) \to 0$ for $x \to \infty$ sufficiently fast, as can be seen from the f sum rule Eq. (21). The exact shape of $s(x)$ depends on the nucleon interaction potential. In particular, the high $x$ behavior is governed by the small-distance regime which is usually dominated by a hard-core repulsion.

Modifications of $s(\omega/T)$ at $\omega \gtrsim T$ do not have a big influence on the loss rate Eq. (17), because of the exponential factor. The finite-width modification is also unimportant as long as $\Gamma_\sigma \lesssim T$, i.e., in the dilute medium. In this regime, we have $\Gamma_\sigma \simeq \Gamma_\sigma^{(1)}$ and $Q_a \simeq Q_a^{(1)} \propto n_b\Gamma_\sigma^{(1)}T^3$ [see Eq. (12)]. For $\Gamma_\sigma \gg T$, in contrast, $Q_a/(n_bT^4)$ would start to decrease with increasing $\Gamma_\sigma$ [26]. This would be the case if $\Gamma_\sigma \simeq \Gamma_\sigma^{(1)}$ up to the highest densities [see Eq. (18)]. However, in Ref. [26] it was argued that $\Gamma_\sigma$ is likely to saturate at some maximum value $\Gamma_\sigma^{\max} \lesssim 150\,\mathrm{MeV}$. This also implies that neutrino opacities are suppressed by less than $\simeq 50\%$ compared to the lowest-order opacities, ensuring consistency of the observed and

simulated cooling time scales for SN 1987A [25]. For $\Gamma_\sigma \lesssim 150\,\mathrm{MeV}$, $Q_a \simeq Q_a^{(1)}$ is a good approximation. For a first improvement to account for saturation of $\Gamma_\sigma$, we therefore set

$$Q_a = Q_a^{(1)}\,\mathrm{Min}\left[1, \frac{\Gamma_\sigma^{\max}}{\Gamma_\sigma^{(1)}}\right] \quad \text{with} \quad \Gamma_\sigma^{\max} \equiv 2\pi W \tag{24}$$

in the numerical simulations, with $Q_a^{(1)}$ taken from Eq. (12). The maximum value of the spin fluctuation rate, $\Gamma_\sigma^{\max}$, is coined in terms of the average interaction energy $W$ of a nucleon in the nuclear medium. This definition is motivated by Eq. (22) and implies the relation $W = -\langle H_T \rangle / (n_b V)$.

We have made no systematic attempt to include the effects of a saturation of nucleon spin fluctuations due to many-body interactions in case of the pion-axion conversion process. However, irrespective of whether the process involves real pions or virtual pions from a bystander nucleon, axions are emitted by the fluctuating nucleon spin whose fluctuation rate $\Gamma_\sigma$ is expected to saturate according to $\Gamma_\sigma^{\max}$ of Eq. (24). Inclusion of saturation effects is therefore likely to leave axion bounds considerably less sensitive to the abundance of pions than suggested by the lowest-order energy-loss rate of Eq. (14).

## IV. AXIONS AND PROTONEUTRON STAR COOLING

### A. Models

In this section we discuss our protoneutron star cooling calculations which were performed with a systematic variation of the axion-nucleon couplings and with different input physics in the neutron star modeling. The considered axion-nucleon coupling constants $g_{ai}$ are of the order of $10^{-10}$ and thus axion opacity plays no role [35].

In our first sequence of cooling models, the loss of energy by nucleon-pair axion bremsstrahlung [Eqs. (12) and (13)] was investigated in dependence of the two parameters $g_{ap}$ and $x \equiv g_{an}/g_{ap}$ which were chosen from the intervals $0 \le g_{ap}/10^{-10} \le 10$ and $-3 \le x \le 3$, respectively. Suppression or saturation of the axion emission rates was not taken into account. The nucleon degeneracy parameter $\xi$ of Eq. (11) was set to 0.5, but comparative calculations with $\xi = 1.0845$ (nondegenerate nucleons) and $\xi = 0$ (very degenerate nucleons) revealed only a very weak dependence of the results on the particular value of $\xi$.

In a second sequence of models we repeated these cooling calculations with many-body effects taken into account according to Eq. (24) where $Q_a^{(1)}$ is from Eq. (12) and $\Gamma_\sigma^{(1)}$ is defined in Eq. (18). The average interaction energy per nucleon, $W$, was chosen to be $W = 10\,\mathrm{MeV}$, corresponding to $\Gamma_\sigma^{\max} \simeq 60\,\mathrm{MeV}$. A finite value of $W$ leads to a saturation of the axion emission rate for large values of $\Gamma_\sigma^{(1)}$, i.e., at high densities and/or high temperatures. Our "standard" case without saturation is formally recovered for $\Gamma_\sigma^{\max} \propto W \to \infty$. We also performed comparative computations for the values $W = 5\,\mathrm{MeV}$ and $W = 20\,\mathrm{MeV}$.

In a third set of models we considered the effects of the presence of a large number of negative pions in the nuclear medium. Pions were included in an ad hoc manner as described in Sect. II B by assuming $0.5 < Y_{\pi^-} < 1$ for the number of $\pi^-$ per nucleon at densities above $\rho_{\mathrm{nuc}}$. The rate of energy loss via the pion-axion conversion reaction is given by Eq. (14).

Because of the 10–50 times larger rate compared to nucleon-nucleon axion bremsstrahlung, a range of coupling parameters $0 \leq \bar{g}_{aN}/10^{-10} \leq 2$ was explored.

In addition to these three sets of models and the variations of $\xi$ and $W$ mentioned above, we replaced the hyperon equation of state (EOS B) by an ordinary $n$-$p$ equation of state (EOS A) in order to reveal the differences for the axion production during the Kelvin-Helmholtz cooling of the protoneutron star when hyperons and $\Delta$-resonances are not present at densities beyond $2\rho_{\rm nuc}$. Furthermore, the influence of a reduction of the neutrino opacity at high densities due to rapid nucleon spin fluctuations [14–16,26] was explored. A suppression factor of 50% was assumed, which is the maximum reduction still allowed by consistency between the SN 1987A neutrino detections and the calculated neutrino signals for axionless cooling models [25]. Finally, the sensitivity of the derived axion mass limits on the mass of the cooling neutron star was tested by performing cooling calculations not only for our standard protoneutron star model with $M_{\rm ns,b} = 1.53\,M_\odot$, but also for models with baryonic masses $M_{\rm ns,b} = 1.30\,M_\odot$, $1.40\,M_\odot$, $1.65\,M_\odot$, and $1.75\,M_\odot$. Like most of the other comparative computations, the simulations with different neutron star masses were done with the reference values $g_{ap} = 1.5 \times 10^{-10}$ and $x = 0$.

### B. Protoneutron Star Evolution without and with Axion Emission

For sufficiently large axion-nucleon coupling the cooling of protoneutron stars is significantly affected by the production of freely escaping axions. We compare here the results for cooling calculations of the $1.53\,M_\odot$ neutron star, once without axions ($g_{ap} = g_{an} = 0$) and another time with the representative choice for the axion coupling constants of $g_{ap} = 1.5\times10^{-10}$ and $x = g_{an}/g_{ap} = 0$. The energy loss rate due to axion emission was prescribed according to Eq. (12), i.e., suppression or saturation of the axion emission at high densities and temperatures was not taken into account. The temperature evolution for the axionless case is shown in Fig. 2, the corresponding information for the case with axions is given in Fig. 3.

The initial temperature profile ($t = 0$) corresponds to the situation a few ten milliseconds after core bounce. The temperature shows a flat hump between the (baryonic) mass coordinates of $M(r) \equiv N_b(r)m \sim 0.3\,M_\odot$ and $\sim 0.9\,M_\odot$ ($N_b(r)$ is the total baryon number inside radius $r$). The temperature in these intermediate layers of the protoneutron star is higher than near the center because of the heating caused by the forming supernova shock. Moreover, as the deleptonization of the protoneutron star progresses, electron degeneracy energy which is released in the process $e^- + p \to n + \nu_e$, is not completely radiated away from the surface of the star by the emission of all kinds of neutrinos. Instead, due to downscattering and multiple absorption and reemission of diffusing neutrinos, a part of this energy stays in the star and leads to heating of the gas. Therefore the temperature in the interior of the star rises during the first $\sim 7\,$s of the evolution (Fig. 2) and the temperature peak advances inward to the center of the star, following the motion of the layer where most of the lepton (electron) loss occurs. At the time when the temperature maximum has reached the center of the star (after $\sim 7\,$s), the chemical potential $\mu_{\nu_e} = \mu_e + \mu_p - \mu_n$ of electron neutrinos has dropped to its final equilibrium value $\mu_{\nu_e} = 0$ that corresponds to deleptonized, neutronized conditions. Now the star begins to cool down essentially coherently by the continuing energy loss due to the emission of neutrino-antineutrino pairs created by thermal processes. After about 38 s the temperatures are below $\sim 3\,$MeV in the whole star.

If axions are produced by nucleon-nucleon bremsstrahlung in significant amounts, two consequences follow for the cooling. On the one hand, the maximum temperature in the star reaches only about 35 MeV at the mass coordinate $M(r) \sim 0.7\,M_\odot$ (Fig. 3). This has to be compared with the peak temperature of $\sim 48$ MeV realized at the center of the star for the case without axion emission (Fig. 2). On the other hand, the temperature starts to drop right from the beginning and already after 18 s the whole star has cooled down to a temperature of less than 3 MeV everywhere. Obviously, axions are very efficient in transporting away the heat produced after the conversion of degenerate electrons into neutrinos.

In Fig. 4 the local energy emission rate due to nucleon-nucleon axion bremsstrahlung is plotted against the enclosed baryonic rest mass $M(r)$ for different times. The axion emission rate per baryon peaks where $\rho T^{3.5}$ has a local maximum and is largest during the first few seconds of the evolution. At later times the temperatures in the star have dropped appreciably and the energy loss in axions is greatly reduced. This is underlined by Fig. 5 which shows the axion luminosity as a function of time in comparison with the combined luminosities of $\nu_e$ and $\bar{\nu}_e$ (denoted by "$L_{\nu_e}$"), the combined luminosities of $\nu_\mu$, $\bar{\nu}_\mu$, $\nu_\tau$ and $\bar{\nu}_\tau$ (labeled by "$L_{\nu_\mu}$"), and the total luminosity for all neutrinos ($L_\nu$). The axion luminosity decreases by an order of magnitude within 5 s, a time after which $L_\nu$ has dropped by only a factor of 3–4. Note that the luminosities in Fig. 5 include reductions due to gravitational redshift and time dilation for an observer at rest at infinity. Since neutrinos diffuse out through the star and decouple from the stellar matter near the surface of the protoneutron star, their luminosities are corrected for the gravitational redshift at the stellar surface which is typically 25% (of the energy measured at infinity). Axions, instead, leave the star from the deep interior where most of the axion production takes place (see Fig. 4) and their typical redshift is 40–50%. Time dilation (i.e., redshift of the inverse time interval or frequency) is accounted for by the same factors. Therefore the amount of energy transported away from the star by axions relative to the energy emitted in neutrinos is larger than suggested by the integration of the luminosities depicted in Fig. 5.

### C. Parameter Studies

Increasing the axion-proton and axion-neutron couplings $g_{ap}$ and $g_{an}$, respectively, leads to a decrease of the energy radiated in neutrinos. Fig. 6 displays the total energies lost by the $1.53\,M_\odot$ protoneutron star in axions ($E_a^0$) and in neutrinos ($E_\nu^0$) as functions of the coupling parameter $g_{ap}$. The nucleon-pair axion bremsstrahlung is again described by Eq. (12). The symbols mark computed models and are connected by cubic spline interpolation. The different lines correspond to the values $x = g_{an}/g_{ap} = 0\,, \pm 0.5\,, \pm 1.0$. The axion energy is larger for larger absolute values of $x$ and a slight difference between the results for positive and negative $x$ (with the values of $E_a^0$ being a bit larger for positive $x$) reflects the asymmetry of the last term in Eq. (12) against changes of the sign of $g_{an}$. In Fig. 6, both $E_a^0$ and $E_\nu^0$ are the energies as measured by a locally inertial observer at rest at the surface of the protoneutron star. The axion energy is therefore corrected for the gravitational redshift between the layers of the axion production and the neutron star surface.

Fig. 7 shows the number of $\bar{\nu}_e$ absorption events predicted for the KII detector, $N_{\rm KII}$, and Fig. 8 the time interval $t_{\rm KII}$ within which 90% of these events are registered. Figs. 9 and 10 give the corresponding information for the IMB detector. Because the fraction of the gravitational binding energy emitted in neutrinos decreases when more energy is carried

away by axions (Fig. 6), all quantities displayed in Figs. 7–10 exhibit a rapid reduction with increasing $g_{ap}$. This reduction is stronger for larger $|x|$. For an axion-proton coupling constant between $1 \times 10^{-10}$ and $2 \times 10^{-10}$, the expected numbers of detector events and the detection times are reduced to about half of the values for the axionless case. While the calculated 11 neutrino events within $\sim 15\,s$ for the $1.53\,M_\odot$ protoneutron star are in reasonable agreement with the KII measurement of SN 1987A neutrinos (11 neutrinos in 12.5 s), the $\sim 6$ predicted IMB events within $\sim 9$ s are clearly on the low side of the detection rate of SN 1987A neutrinos in IMB (8 neutrinos in 5.6 s). This trend of our results is also present for supernova models of other groups and reflects the marginal consistency observed between the IMB and KII neutrino data: For the $\bar{\nu}_e$ emission characteristics (spectrum and luminosity) deduced from the KII measurement, one would expect a much smaller number of IMB events, or, inversely, $\bar{\nu}_e$ emission that has caused the 8 events in IMB should have produced a much larger signal in the KII detector (see, e.g., [36]).

If axion emission is absent, the expected event numbers $N_{\rm KII}$ and $N_{\rm IMB}$ as well as the detection times $t_{\rm KII}$ and $t_{\rm IMB}$ are slowly increasing with the mass of the protoneutron star [25]. Between $M_{\rm ns,b} = 1.30\,M_\odot$ and $M_{\rm ns,b} = 1.75\,M_\odot$, $N_{\rm KII}$ and $N_{\rm IMB}$ roughly double, while $t_{\rm KII}$ increases by a factor of 2.5 and $t_{\rm IMB}$ by about 60%, as can be seen in Table 1 of [25]. When axions are produced in the stars by nucleon-pair bremsstrahlung [Eq. (12)] with axion-proton coupling $g_{ap} = 1.5 \times 10^{-10}$ and axion-neutron coupling $g_{an} = 0$ (i.e., $x = 0$), the results for different neutron star masses are obtained as shown in Fig. 11. All four quantities reveal a very weak dependence on the baryonic mass of the neutron star. For the used values of the axion-nucleon coupling constants, we find $N_{\rm KII} \simeq 5$, $N_{\rm IMB} \simeq 3$, $t_{\rm KII} \simeq 6$ s, and $t_{\rm IMB} \simeq 3.8$ s in all cases. Independent of the protoneutron star mass, these results are about half of the values found for the case of the $1.53\,M_\odot$ star without axion emission. The same inert behavior is also observed for the average energies of the electron antineutrinos captured in the two detectors: $\langle\epsilon_{\rm KII}\rangle \simeq 23.7$ MeV and $\langle\epsilon_{\rm IMB}\,\rangle \simeq 34.5$ MeV. In more massive protoneutron stars the temperature and density become higher; this causes enhanced emission of axions so that a smaller fraction of the released gravitational binding energy ends up in neutrinos. The weak variation of the expected neutrino signals suggests that the additional gravitational energy release associated with a larger neutron star mass is essentially completely carried away by axions.

Our study with varied parameters $g_{ap}$ and $x$, based on the $1.53\,M_\odot$ protoneutron star model, was repeated for the case that the axion emission rate saturates at high densities and temperatures (see Sect. III C). Employing Eq. (24) with $Q_a^{(1)}$ from Eq. (12) (with $\xi = 0.5$) and $\Gamma_\sigma^{(1)}$ from Eq. (18), the axion emission rate reaches its saturation level when $\rho_{14} T_{10}^{1/2} \gtrsim 2W(10\,{\rm MeV})^{-1}$. For an average interaction energy per nucleon of $W = 10$ MeV we found that the corresponding reduction of the axion production increases the predicted number of neutrino events $N_{\rm KII}$ and $N_{\rm IMB}$ by roughly 40% compared to the number of expected events for the "naive" (unsaturated) case for which formally $W \to \infty$. This trend turned out to be even somewhat stronger for the detection times $t_{\rm KII}$ and $t_{\rm IMB}$ where the increase was about 60%. For $W = 20$ MeV the increase was $\sim 20$% in the event numbers and $\sim 30$% in the detection times, and for $W = 5$ MeV the event numbers and detection times rose by 60% and 80%, respectively.

Taking into account the possible existence of a large number of negative pions at high densities in the simple way described in Sect. II B and using the energy loss rate due to pion-axion conversion as given in Eq. (14), a reduction of the predicted detector response ($N_{\rm KII}$, $N_{\rm IMB}$, $t_{\rm KII}$ and $t_{\rm IMB}$) to 75% of the values for the axionless case occurred for $\bar{g}_{aN} \simeq$

$0.15 \times 10^{-10}$. A reduction by 50% was seen when $\bar{g}_{aN} = (0.30 \ldots 0.40) \times 10^{-10}$, and only 25% of the neutrino events were measured in roughly four times shorter time when $\bar{g}_{aN}$ was between $0.75 \times 10^{-10}$ and $1.0 \times 10^{-10}$. Of course, the neutrino emission characteristics of the simulated protoneutron stars vary with time. Therefore, the detection rates in KII and IMB are not constant, and, correspondingly, the values of the axion-pion coupling $\bar{g}_{aN}$ which lead to a certain reduction are somewhat different for the two experiments and also for the event numbers and detection times.

Our results exhibit an extremely weak dependence on the choice of the nucleon degeneracy parameter $\xi$ of Eq. (11). Changing $\xi$ from 0 (degenerate nucleons) to 1.0845 (nondegenerate nucleons) leads to an increase of $N_{\rm KII}$ by $\sim 0.5$ events and to a detection time $t_{\rm KII}$ that is $\sim 0.5\,$s longer. For the IMB detector the corresponding numbers are $\sim 0.25$ events and $\sim 0.25\,$s, respectively. A larger value for $\xi$ reduces the energy-loss rate by axion emission [Eq. (12)], but the particular choice of $\xi$ is irrelevant at the level of accuracy implied by the sparseness of the neutrino data of SN 1987A.

Replacing the hyperonic EOS B by the $n$-$p$ EOS A in our $1.53\,M_\odot$ protoneutron star model leads to essentially no change in the predicted neutrino signals. Hyperonization plays an important role only in stars with baryonic masses $\gtrsim 1.70\,M_\odot$ where the density in a larger part of the star is high enough to favor the production of hadronic states other than $n$ and $p$ (see [22] and compare also models S4BH_0 and S4AH_0 of Table 1 in [25]).

A suppression of the neutrino opacities relative to their "standard" values, e.g., by the many-body effects discussed in Sect. III C, can have an important impact on the predicted neutrino signal [25] and thus on the allowed range of axion-nucleon couplings deduced from the SN 1987A neutrino data. As a test, we reduced the axial vector contributions of neutral- and charged-current processes by about 50% (i.e., we chose $a = 0.5$, see [25]) in the case of the $1.53\,M_\odot$ protoneutron star with axion emission prescribed according to Eq. (12) and $g_{ap} = 1.5 \times 10^{-10}$ and $x = 0$. The characteristics of the detector signals change in the same way as found for the axionless case in [25]. A 50% reduction of the neutrino opacities leads to an increase of the predicted numbers of neutrino events $N_{\rm KII}$ and $N_{\rm IMB}$ by $\sim 2.2$, but the detection times $t_{\rm KII}$ and $t_{\rm IMB}$ drop by about 25%. The mean energies of $\bar{\nu}_e$ registered by the detectors rise by roughly 2 MeV. Since these changes are not dramatic, it is clear that even a 50% reduction of the neutrino opacity in the protoneutron star will not completely alter conclusions on the axion production drawn from a comparison of theoretical neutrino signals with the SN 1987A neutrino data. Although the increase of the number of detector events in case of a lower neutrino opacity can somehow compensate for the effects of axion emission, the detection times shrink *both* by a reduction of the neutrino cross sections *and* by the additional axion cooling of the star. Therefore we conclude that a value of the neutrino opacity that is lower than the "standard" one can hardly lead to a restoration of the compatibility between the SN 1987A neutrino signal and the signal predicted in case of strong axion emission.

### D. Excluded axion couplings and axion mass limits

The cooling sequences of the $1.53\,M_\odot$ protoneutron star model for varied axion-nucleon coupling parameters $g_{ap}$ and $x = g_{an}/g_{ap}$ are used to construct exclusion curves in the $x$-$g_{ap}$-space. The sensitivity against changes of the axion couplings was found to be somewhat different for predicted event numbers and detection time scales. Nevertheless, it is safe to

claim that consistency between the theoretical neutrino signal and the SN 1987A neutrino data requires that $N_{\rm KII,IMB} \gtrsim \frac{1}{2} N^{\rm s}_{\rm KII,IMB}$ and $t_{\rm KII,IMB} \gtrsim \frac{1}{2} t^{\rm s}_{\rm KII,IMB}$ when $N^{\rm s}_{\rm KII,IMB}$ and $t^{\rm s}_{\rm KII,IMB}$ are the expected signal parameters for the axionless "standard" $1.53\,M_\odot$ protoneutron star model. According to this criterion, the bell-shaped curves in Fig. 12 separate allowed from forbidden regions. The lower curve corresponds to the case where the energy loss in axions is described by Eq. (12), the upper curve represents the case where saturation of axion emission is included [Eq. (24)] with an average interaction energy per nucleon of $W = 10\,{\rm MeV}$. The values of the upper curve can be obtained from those of the lower curve by scaling with a factor of about 1.9.

On the hatched sides above the curves the axion-nucleon couplings are so large that more than about half of the gravitational binding energy of the neutron star is emitted in axions and only less than half in neutrinos (compare Fig. 6). There is only a slight asymmetry between positive and negative values of $x$ which is caused by the minor asymmetry of the third term of $Q_a^{(1)}$ in Eq. (12) against changes of the sign of $g_{an}$. Obviously, the contribution of the asymmetric term $\propto g_{an} g_{ap}$ is rather small. For this reason, the lower curve of Fig. 12 can be pretty well fitted by the relation $g_{ap}^2 + 2 g_{an}^2 \simeq (1.5 \times 10^{-10})^2$ which means that the excluded values of the axion-nucleon coupling constants lie outside of an ellipse with semiaxes $1.5 \times 10^{-10}$ and $(1.5/\sqrt{2}) \times 10^{-10}$ in the $g_{ap}$-$g_{an}$-plane.

The deduced limits for allowed values of the coupling constants $g_{ap}$ and $x = g_{an}/g_{ap}$ might be sensitive to the protoneutron star mass. This was tested by varying the baryonic mass of the protoneutron star for $g_{ap} = 1.5 \times 10^{-10}$ and $x = 0$. In case of the $1.53\,M_\odot$ model this pair of values ($x$,$g_{ap}$) lies on the lower exclusion curve of Fig. 12. The results of such a study are displayed in Fig. 11. The observed inertia of the predicted neutrino signal against changes of the mass of the axion-emitting star suggests that the exclusion curves should not depend strongly on the (unknown) exact mass of the neutron star born in SN 1987A.

Taking into account the possible existence of a large number of negative thermal pions in the protoneutron star in the simple way described in Sect. II B, we find that the rapid energy loss by axions emitted in pion-axion conversion processes [Eq. (14)] excludes couplings of roughly $\bar{g}_{aN} \gtrsim (0.30 \ldots 0.40) \times 10^{-10}$. This assumes a perturbative treatment of the emission processes and neglects possible saturation effects. Since for typical conditions in the supernova core the perturbative energy emission rate by pion-axion conversion is approximately 10–20 times larger than the lowest-order energy-loss rate for the nucleon-nucleon axion bremsstrahlung, the bound on the coupling constant $\bar{g}_{aN}$ would be 3–5 times more stringent than the limit on $g_{ap}$ in the perturbative case.

With these limits on the axion coupling parameters $g_{ap}$, $g_{an}$ (or, equivalently, $x$), and $\bar{g}_{aN}$, upper limits on the axion mass can be derived from Eqs. (3) and (15) when use is made of the experimental values for the dimensionless couplings $C_p$ and $C_n$ (see Sect. II A) collected in Fig. 1, and Eq. (1) is employed to relate the PQ scale (or axion decay constant) $f_a$ with the axion mass $m_a$. From Eqs. (3) and (1) one finds

$$\frac{m_a}{10^{-3}\,{\rm eV}} \lesssim \frac{0.66}{C_p}\,\frac{g_{ap}^{\rm max}}{10^{-10}}\,, \tag{25}$$

and from Eqs. (15) and (1) one obtains

$$\frac{m_a}{10^{-3}\,{\rm eV}} \lesssim \frac{0.66}{C_p}\left(\frac{1}{2} + \frac{x^2}{2} - \frac{x}{3}\right)^{-1/2}\,\frac{\bar{g}_{aN}^{\rm max}}{10^{-10}}\,. \tag{26}$$

Here $g_{ap}^{\rm max}$ and $\bar{g}_{aN}^{\rm max}$ are the maximum values of the axion couplings allowed by the SN 1987A neutrino detections, and $C_p = g_{ap}/[m_p/(f_{\rm PQ}/N)]$ and $x$ correspond to the pair of coordinate values of a particular chosen point in Fig. 1. Note that $g_{ap}^{\rm max}$ as a function of $x$ describes the (lower) exclusion curve in Fig. 12.

The upper bounds of the axion mass deduced for the points of Fig. 1 by this procedure are plotted in Fig. 13. Above a line connecting the point $(g_{an}/g_{ap}, m_a/[10^{-3}\,{\rm eV}]) = (-1, 1)$ with the point $(3, 5)$, Fig. 13 shows the results for the "standard" case without pions, whilst below this line the dots represent the mass limits for the case with pion-axion conversion. In both cases saturation effects have been neglected. The latter case yields axion mass limits that are stronger by a factor of almost four. As was mentioned in Sect. III C, the inclusion of saturation effects is expected to lead to limits that are less sensitive to the presence of pions.

## V. SUMMARY

We have re-examined the stringent limit on the axion mass inferred from neutrino emission by SN 1987A, in the light of a possible suppression of axion emission by the many-body effects of nucleon spin fluctuations and additional emission processes involving pions, taking into account the latest determinations of axial-vector current couplings to nucleons. The suppression of axion emission due to many-body effects degrades previous limits by a factor of about 2. Emission processes involving thermal pions can strengthen the limits by a factor of 3–4, if saturation effects on the nucleon spin fluctuations are neglected, whereas inclusion of such effects tends to make the limits less sensitive to pion abundances. The resulting axion mass limit depends upon its precise couplings, ranging from $0.5 \times 10^{-3}\,{\rm eV}$ to $6 \times 10^{-3}\,{\rm eV}$. Our results are consistent with previous limits [10], though more precisely stated. Fig. 12 shows our limit on the axion-proton coupling as a function of the ratio of the axion-neutron to axion-proton couplings, and Fig. 13 shows the mass limit as a function of this same ratio.

To test the stability of the deduced axion mass limits against uncertainties of the stellar models and of the description of the input physics, we performed a large number of comparative computations. It turned out that neither a change of the nucleon degeneracy parameter $\xi$ of Eq. (11) nor a reduction of the neutrino opacity to 50% of its standard value lead to major changes of our conclusions. There are differences of our work compared to previous work by Burrows et al. [10] concerning the protoneutron star modeling, namely we used different equations of state and did not take into account accretion of matter onto the nascent neutron star.

Two different equations of state were used in the presented models, an *n-p* equation of state and an equation of state where hyperons occur as additional hadronic degrees of freedom at densities beyond about two times nuclear matter density [23]. For neutron stars with baryonic masses $\lesssim 1.70\,M_\odot$ hyperons are abundant only in a relatively small central core region of the forming neutron star and therefore do not dramatically change the cooling and neutrino emission of the star. Similarly, the axion emission was found to be affected only at a minor level by the presence of hyperons.

The amount of material possibly accreted onto the protoneutron star during the first moments of the supernova explosion and the corresponding accretion rate as a function of time are rather uncertain and must depend on the structure of the progenitor star and on the details of the still incompletely understood explosion mechanism of Type II supernovae.

Instead of introducing new free parameters to model accretion, we tried to account for the unknown amount of accreted matter by performing cooling simulations for protoneutron star models with baryonic masses between $1.3\,M_\odot$ and $1.75\,M_\odot$. Interestingly, the higher temperatures in more massive stars lead to enhanced axion emission that carries away a larger fraction of the gravitational binding energy that is released during the cooling of the star. Therefore the predicted neutrino signals in the KII and IMB detectors and thus the axion mass limits deduced from the SN 1987A neutrino data should be rather insensitive to the exact mass of the protoneutron star formed in SN 1987A. Including accretion as in Burrows et al. [10] raises the total neutrino luminosity above the contribution from the core and leads to additional events in the detectors which are essentially unaffected by the emission of axions. Therefore the event numbers $N_{\rm KII}$ and $N_{\rm IMB}$ in reference [10] were found to drop somewhat less strongly with increasing axion-nucleon coupling than they do in case of our models.

## ACKNOWLEDGMENTS.

We thank Donald Q. Lamb and G. Raffelt for many valuable discussions and comments. Useful remarks by M. Ruffert are also acknowledged. WK and HTJ are very grateful to N.K. Glendenning for providing them with the tables of his equations of state. They also want to thank J.R. Wilson for the data of the protoneutron star from one of his supernova simulations, which was used to construct some of the initial models for the investigations. This work was supported by the DoE (at Chicago and Fermilab), by the NASA (at Fermilab by grant NAG 5-2788), and by the "Sonderforschungsbereich 375-95 für Astro-Teilchenphysik" of the Deutsche Forschungsgemeinschaft (at Garching). For a part of the work done during a stay at the University of Chicago, HTJ acknowledges support by the NSF grant AST 92-17969, by the NASA grant NAG 5-2081, and by an Otto Hahn Postdoctoral Scholarship of the Max-Planck-Society. The computations were performed on the CRAY-YMP 4/64 and Cray-EL98 4/256 of the Rechenzentrum Garching.

# REFERENCES


[1] R. D. Peccei and H. R. Quinn, Phys. Rev. Lett. **38**, 1440 (1977) and Phys. Rev. D **16**, 1791 (1977).

[2] S. Weinberg, Phys. Rev. Lett. **40**, 223 (1978); F. Wilczek, *ibid* **40**, 279 (1978).

[3] See e.g., M. S. Turner, Phys. Rep. **197**, 67 (1990); G. G. Raffelt, *ibid* **198**, 1 (1990).

[4] J. Preskill, M. Wise and F. Wilczek, Phys. Lett. B **120**, 127 (1983); L. Abbott and P. Sikivie, *ibid*, 133 (1983); M. Dine and W. Fischler, *ibid*, 137 (1983).

[5] M. S. Turner, Phys. Rev. D **33**, 889 (1986).

[6] See e.g., S. Dodelson, E. Gates and M. S. Turner, astro-ph/9603081 (1996).

[7] J. Ipser and P. Sikivie, Phys. Rev. Lett. **50**, 925 (1983); M. S. Turner, F. Wilczek, and A. Zee, Phys. Lett. B **125**, 35 (1983); **125**, 519E (1983).

[8] L. J. Rosenberg, Particle World **4**, 3 (1995).

[9] M. S. Turner, Phys. Rev. Lett. **60**, 1797 (1988); G. G. Raffelt and D. Seckel, *ibid*, 1793 (1988); R. Mayle et al., Phys. Lett. B **203**, 188 (1988) and **219**, 515 (1989).

[10] A. Burrows, R. P. Brinkmann, and M. S. Turner, Phys. Rev. D **39**, 1020 (1989).

[11] K. Hirata et al., Phys. Rev. Lett. **58**, 1490 (1987).

[12] R. M. Bionta et al., Phys. Rev. Lett. **58**, 1494 (1987).

[13] See e.g., A. Burrows, Ann. Rev. Nucl. Part. Sci. **40**, 181 (1990); or D. N. Schramm and J. Truran, Phys. Rep. **189**, 89 (1990).

[14] G. G. Raffelt and D. Seckel, Phys. Rev. Lett. **67**, 2605 (1991).

[15] G. G. Raffelt and D. Seckel, Phys. Rev. D **52**, 1780 (1995).

[16] H.-Th. Janka, W. Keil, G. G. Raffelt, and D. Seckel, Phys. Rev. Lett. **76**, 2621 (1996).

[17] R. Mayle, D. N. Schramm, M. S. Turner, and J. R. Wilson, Phys. Lett. B **317**, 119 (1993); M. S. Turner, Phys. Rev. D **45**, 1066 (1992).

[18] M. Dine, W. Fischler, and M. Srednicki, Phys. Lett. B **104**, 199 (1981); A. P. Zhitnitskii, Yad. Fiz. **31**, 497 (1980) [Sov. J. Nucl. Phys. **31**, 260 (1980)].

[19] J. Kim, Phys. Rev. Lett. **43**, 103 (1979); M. A. Shifman, A. I. Vainshtein, and V. I. Zakharov, Nucl. Phys. **B166**, 493 (1980).

[20] J. Ellis and M. Karliner, *Lectures at the International school on Nucleon Spin Structure*, Erice 1995, CERN preprint TH/95-334, hep-ph/9601280, and references therein.

[21] J. R. Wilson and R. W. Mayle, in: "The Nuclear Equation of State, Part A", Eds. W. Greiner and H. Stöcker, Plenum Press, New York, p. 731 (1989); J. R. Wilson, personal communication (1989).

[22] W. Keil and H.-Th. Janka, Astron. Astrophys. **296**, 145 (1995).

[23] N. K. Glendenning, Astrophys. J. **293**, 470 (1985).

[24] R. W. Mayle, M. Tavani and J. R. Wilson, Astrophys. J. **418**, 398 (1993).

[25] W. Keil, H.-Th. Janka, and G. Raffelt, Phys. Rev. D **51**, 6635 (1995).

[26] G. Sigl, Phys. Rev. Lett. **76**, 2625 (1996).

[27] S. Reddy and M. Prakash, astro-ph/9610115, and references therein.

[28] B. L. Friman and O. V. Maxwell, Astrophys. J. **232**, 541 (1979).

[29] N. Iwamoto, Phys. Rev. Lett. **53**, 1198 (1984).

[30] R. P. Brinkmann and M. S. Turner, Phys. Rev. D **38**, 2338 (1988).

[31] J. D. Bjorken and S. D. Drell, "Relativistic Quantum Mechanics", McGraw-Hill, 1964.

[32] G. Raffelt, "Stars as Laboratories for Fundamental Physics", The University of Chicago Press, 1996.

[33] L. D. Landau and I. Ja. Pomeranchuk, Dokl. Akad. Nauk SSSR **92**, 535 (1953); **92**, 735 (1953); E. L. Feinberg and I. Ja. Pomeranchuk, Nuovo Cimento Suppl. **3**, 652 (1956).

[34] J. Knoll and D. M. Voskresensky, Phys. Lett. B **351**, 43 (1995).

[35] A. Burrows A., T. Ressell and M.S. Turner, Phys. Rev. D **42**, 3297 (1990).

[36] H. Suzuki, PhD Thesis, University of Tokyo (1989).

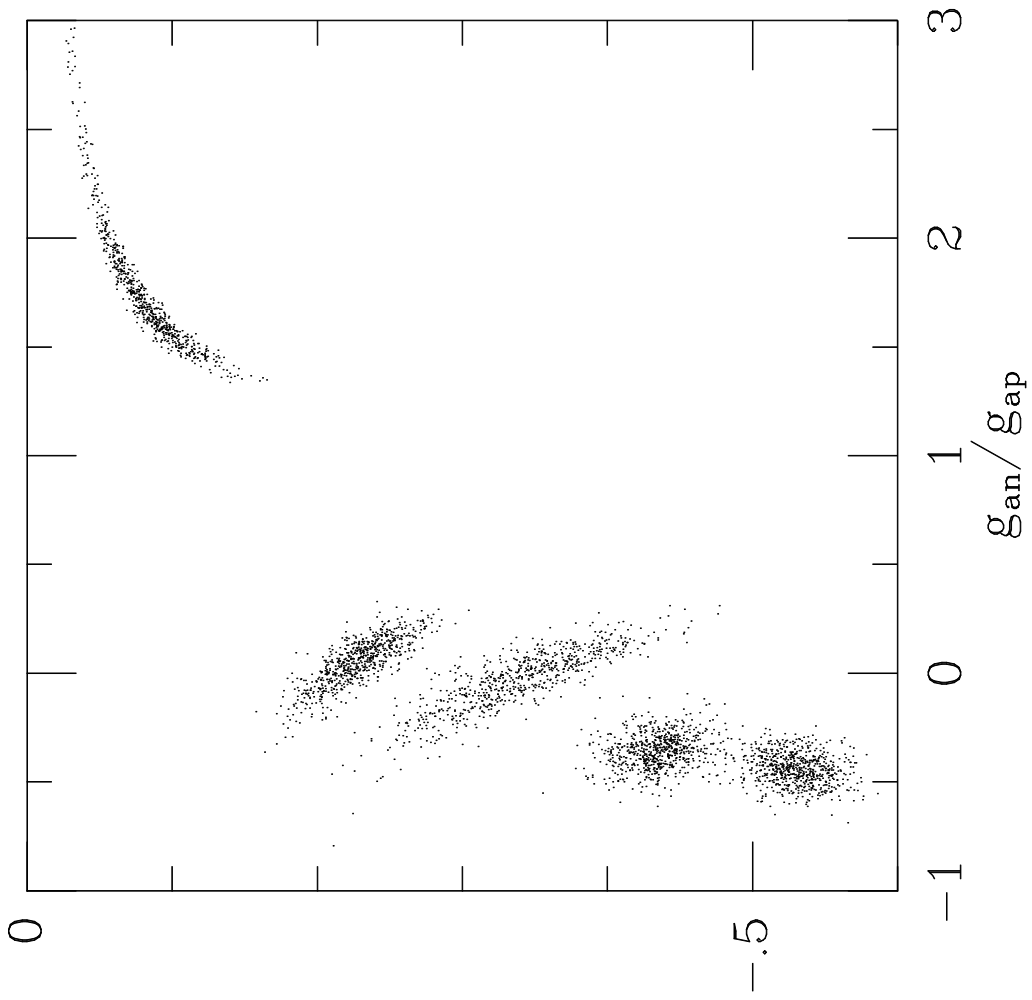


FIG. 1. Scatter plot of the axion-proton coupling and the ratio of the axion-neutron to axion-proton coupling for different axion models allowing for the uncertainties in $\Delta q$; from the bottom left to the top right, $\beta = 0$, $\beta = 27°$, KSVZ, $\beta = 54°$, and $\beta = 81°$. Note that the axion-neutron coupling is much smaller than the axion-proton coupling for the KVSZ axion and for the DFSZ axion when $\beta \sim 45°$.

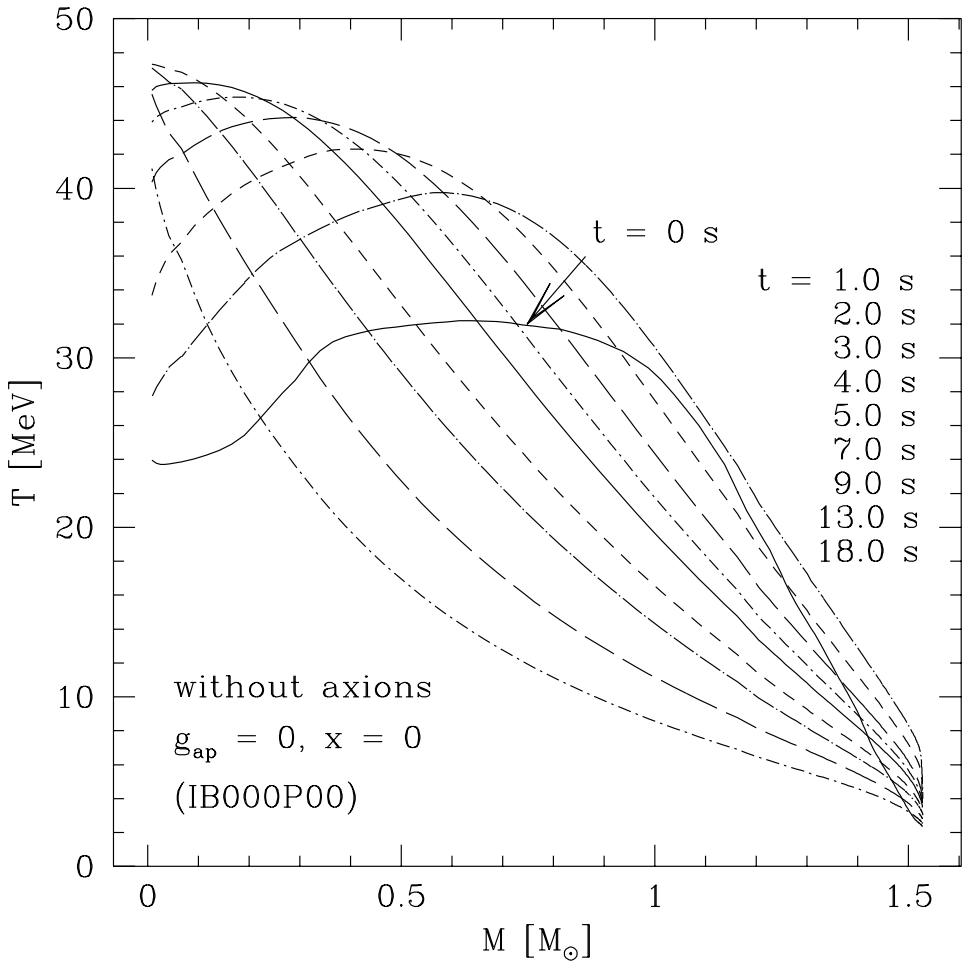


FIG. 2. Temperature evolution of a $1.53\,M_\odot$ protoneutron star without axion emission. The temperature profiles are plotted against the enclosed baryonic rest mass $M(r) = N_b(r)m$ (in solar masses; $m$ is the common nucleon mass) for different times from the start of the computation shortly after the formation of the protoneutron star. For time $t = 0$ the curve is labeled, the other times are listed according to the order of the corresponding curves (from top to bottom at $M = 1\,M_\odot$). The interior of the star heats up first due to the conversion of lepton degeneracy energy into thermal energy, but finally cools.

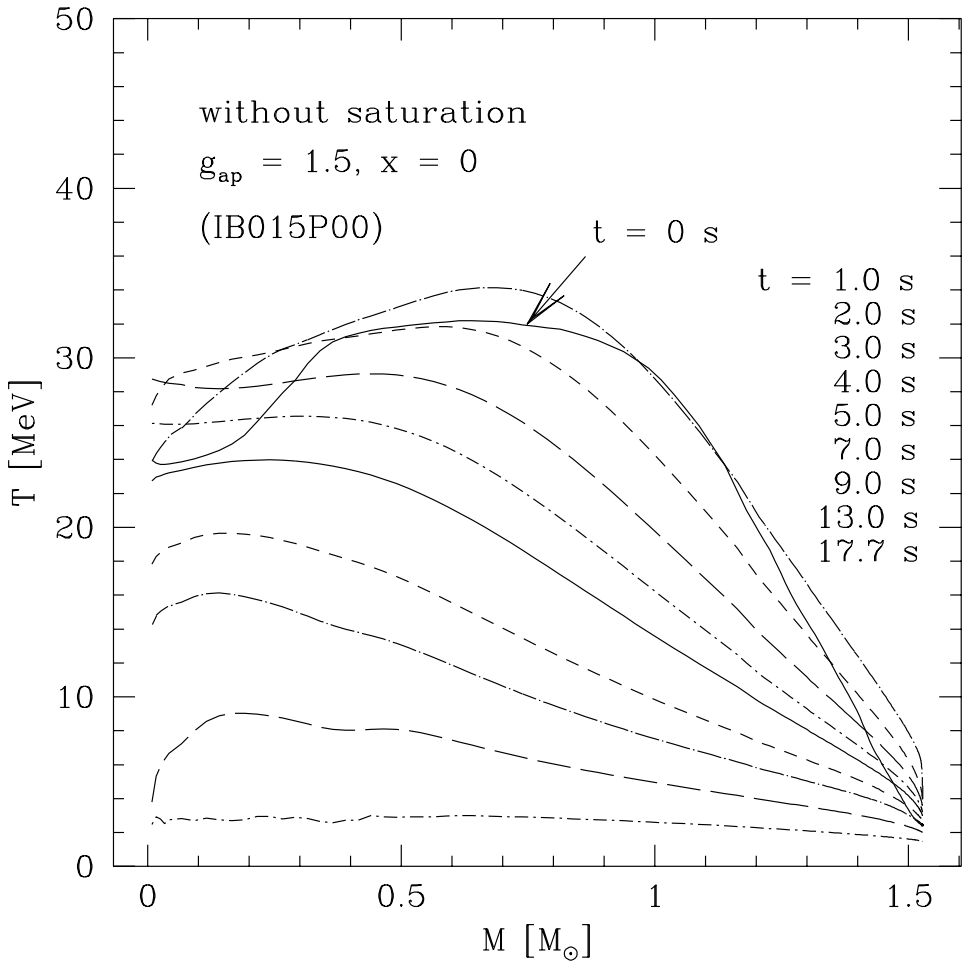


FIG. 3. Temperature profiles of a $1.53\,M_\odot$ protoneutron star vs. enclosed baryonic mass for different times. Axion production via nucleon-pair bremsstrahlung is included with axion coupling constants $g_{ap} = 1.5 \times 10^{-10}$ and $x = g_{an}/g_{ap} = 0$. The star cools much faster than in Fig. 2.

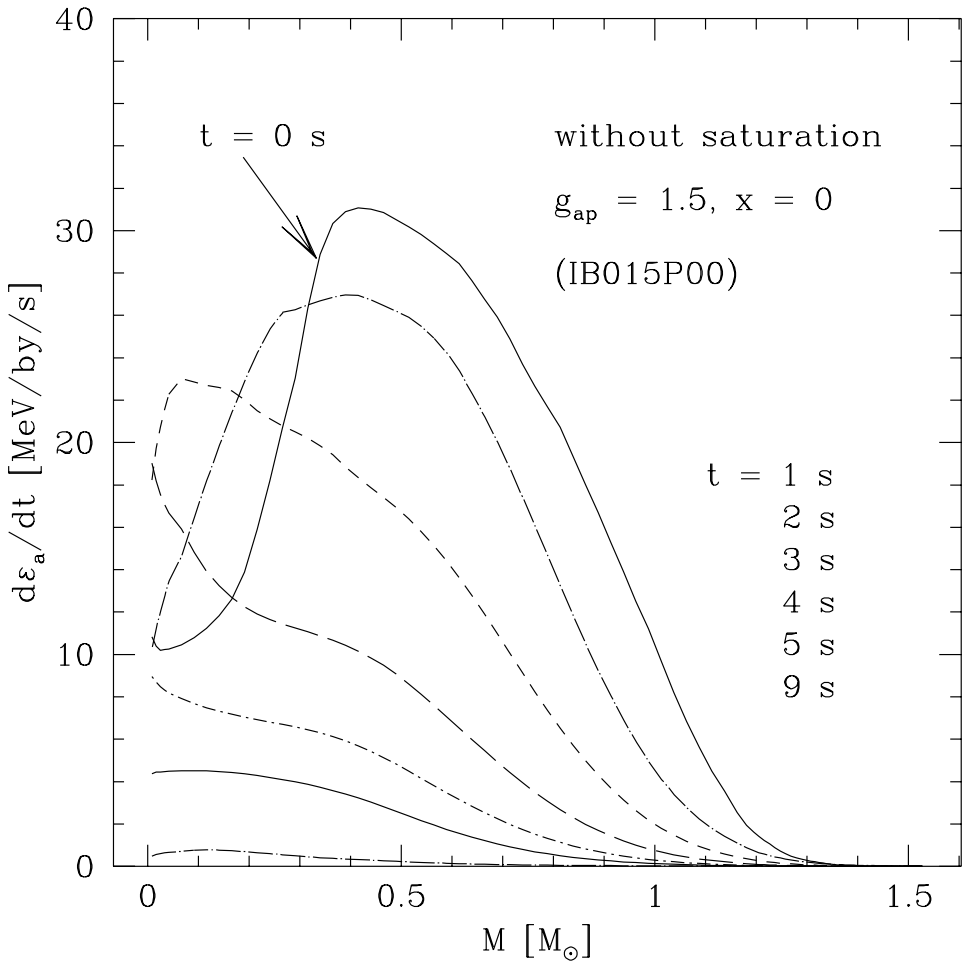


FIG. 4. Local energy production rate per baryon due to nucleon-nucleon bremsstrahlung emission of axions [Eq. (12)] with coupling constants $g_{ap} = 1.5 \times 10^{-10}$ and $x = g_{an}/g_{ap} = 0$. The profiles are plotted against the baryonic mass coordinate of a $1.53\,M_\odot$ protoneutron star for different times after the start of the simulation (the times are listed according to the order of the curves at $M = 0.5\,M_\odot$). The energy production per baryon roughly peaks where the product $\rho T^{3.5}$ reaches a maximum.

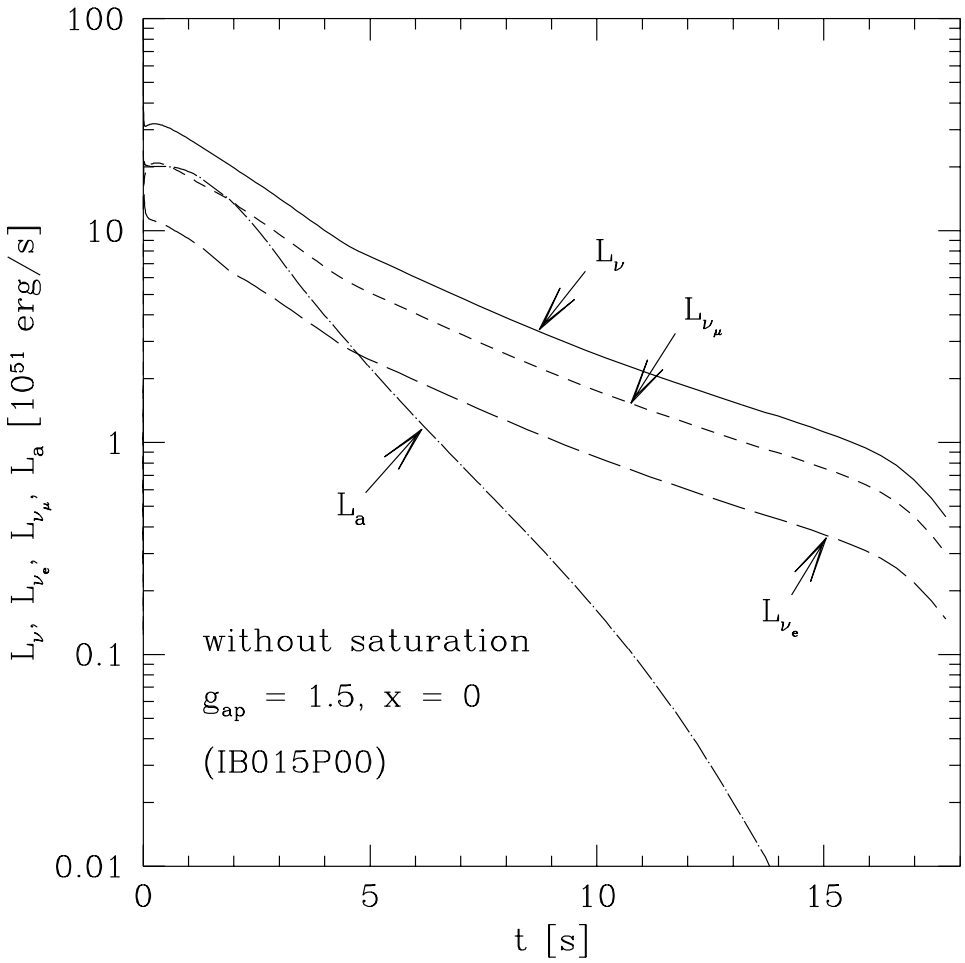


FIG. 5. Electron neutrino plus electron antineutrino luminosity (labeled by $L_{\nu_e}$), sum of all luminosities of heavy lepton neutrinos (labeled by $L_{\nu_\mu}$), total neutrino luminosity $L_\nu$, and axion luminosity $L_a$ as functions of time during the cooling of a $1.53\,M_\odot$ protoneutron star for axion-proton coupling $g_{ap} = 1.5 \times 10^{-10}$ and axion-neutron coupling $g_{an} = 0$. The luminosities are redshifted as measured by an observer at rest at infinity. The axion luminosity drops by an order of magnitude within 5 s, whereas the neutrino emission decreases less rapidly.

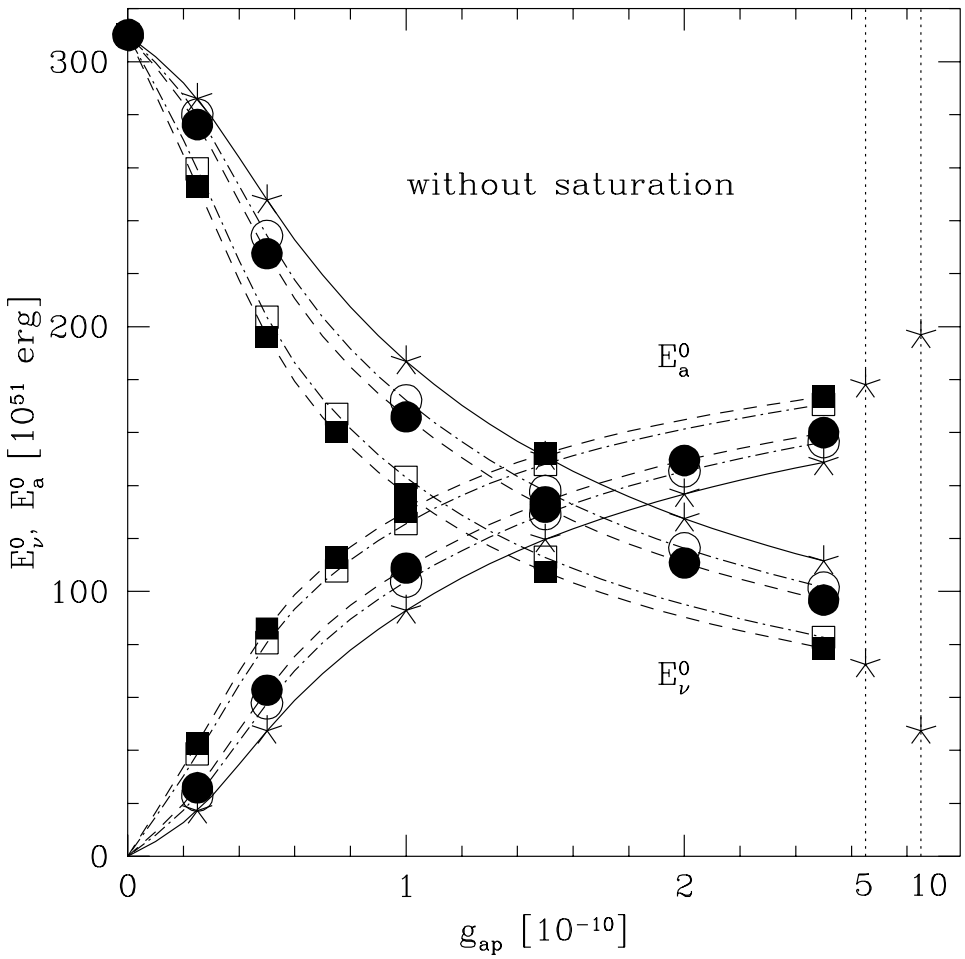


FIG. 6. Energy loss of a $1.53\,M_\odot$ protoneutron star in neutrinos ($E^0_\nu$) and in axions ($E^0_a$) for different combinations of values of the axion-proton coupling $g_{ap}$ and axion-neutron coupling $g_{an}$ in Eq. (12). The energies are given as measured by a locally inertial observer at the surface of the neutron star. The symbols mark computed models, the interpolation is done by cubic splines. The curves through the asterisks correspond to the case $x = g_{an}/g_{ap} = 0$, the circles to the cases $x = \pm 0.5$, and the squares to $x = \pm 1.0$. Filled symbols mark positive, open symbols negative values of $x$.

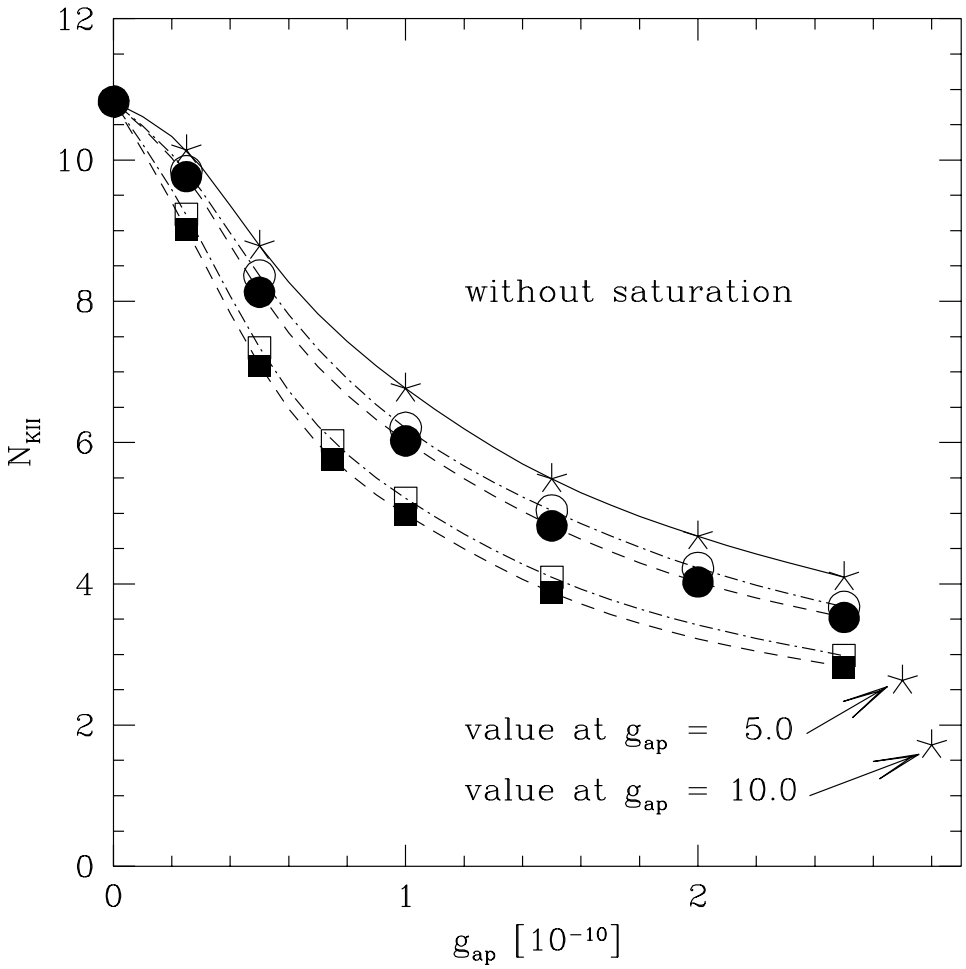


FIG. 7. Prediced number of $\bar{\nu}_e$ absorption events in the KII detector for a $1.53\,M_\odot$ proto-neutron star as a function of the axion-proton coupling $g_{ap}$. The symbols correspond to computed models and the different curves represent different values of $x = g_{an}/g_{ap}$ (see Fig. 6).

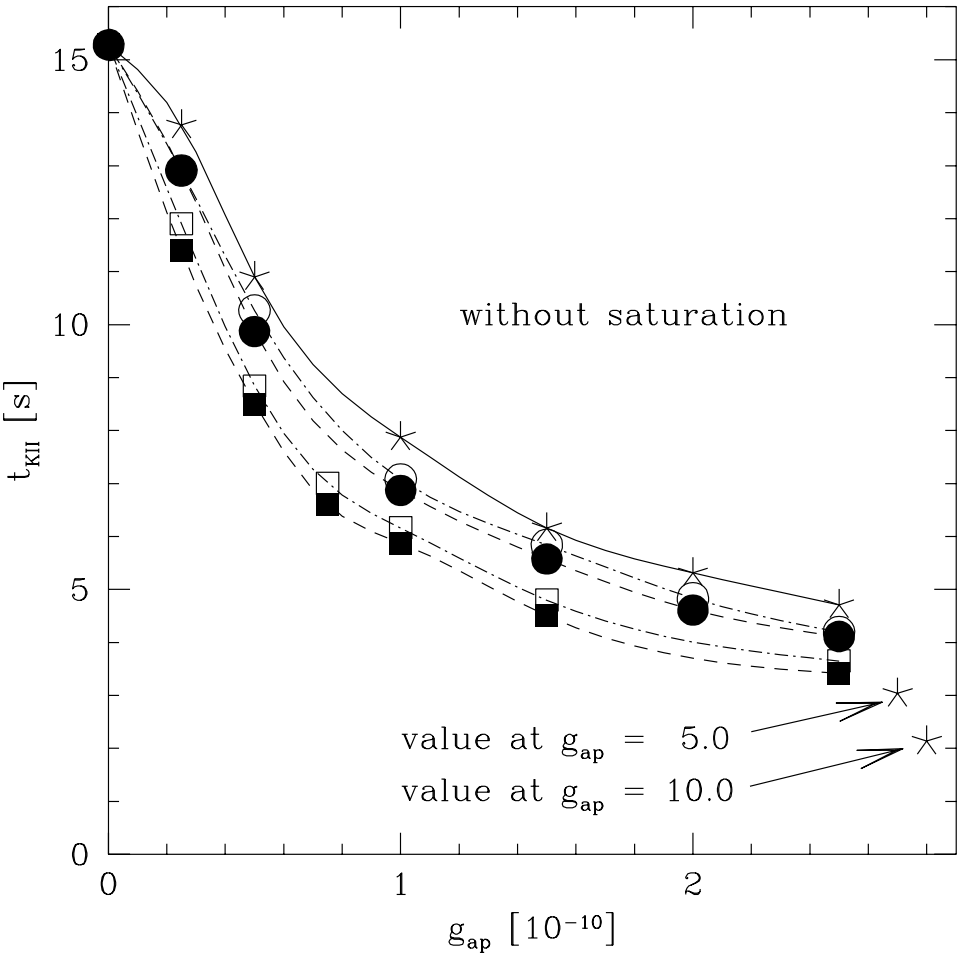


FIG. 8. Time intervals $t_{\rm KII}$ where 90% of the predicted $\bar{\nu}_e$ capture events in the KII detector happen for a protoneutron star with a baryonic mass of $1.53\,M_\odot$ and for different combinations of values of $g_{ap}$ and $x = g_{an}/g_{ap}$. The meaning of the symbols is the same as in Fig. 6.

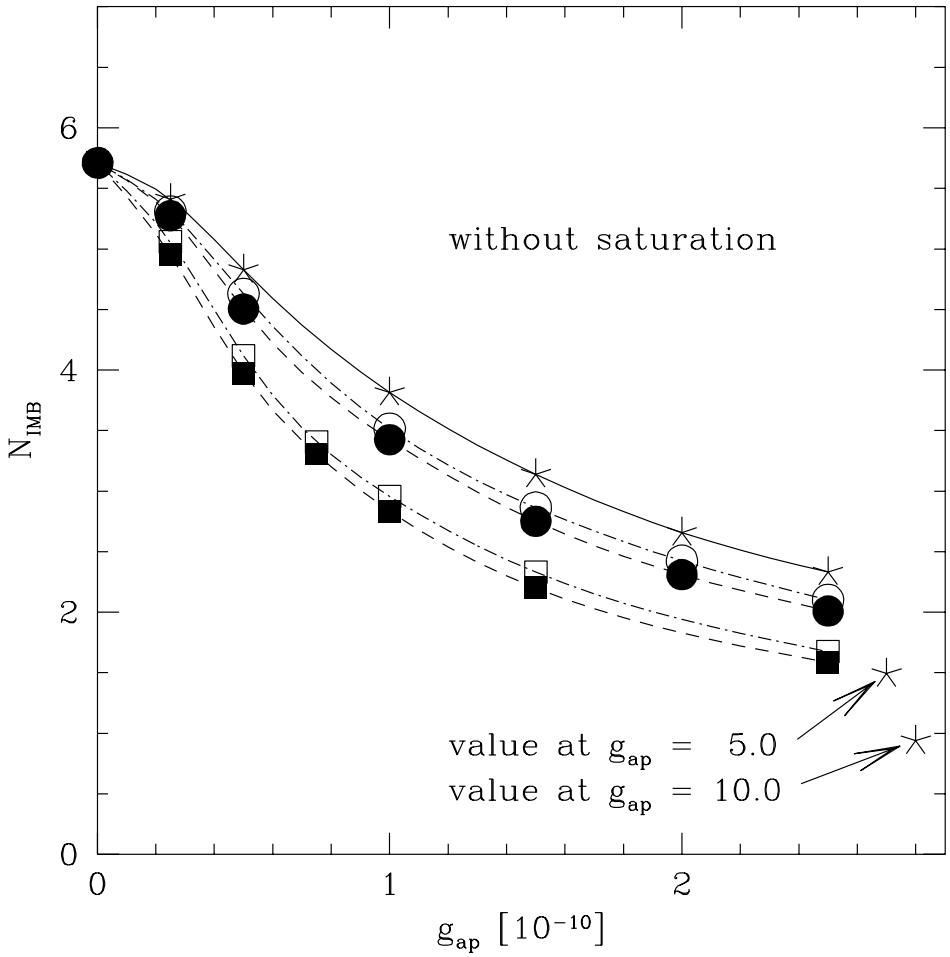


FIG. 9. Same as Fig. 7, but for the IMB detector.

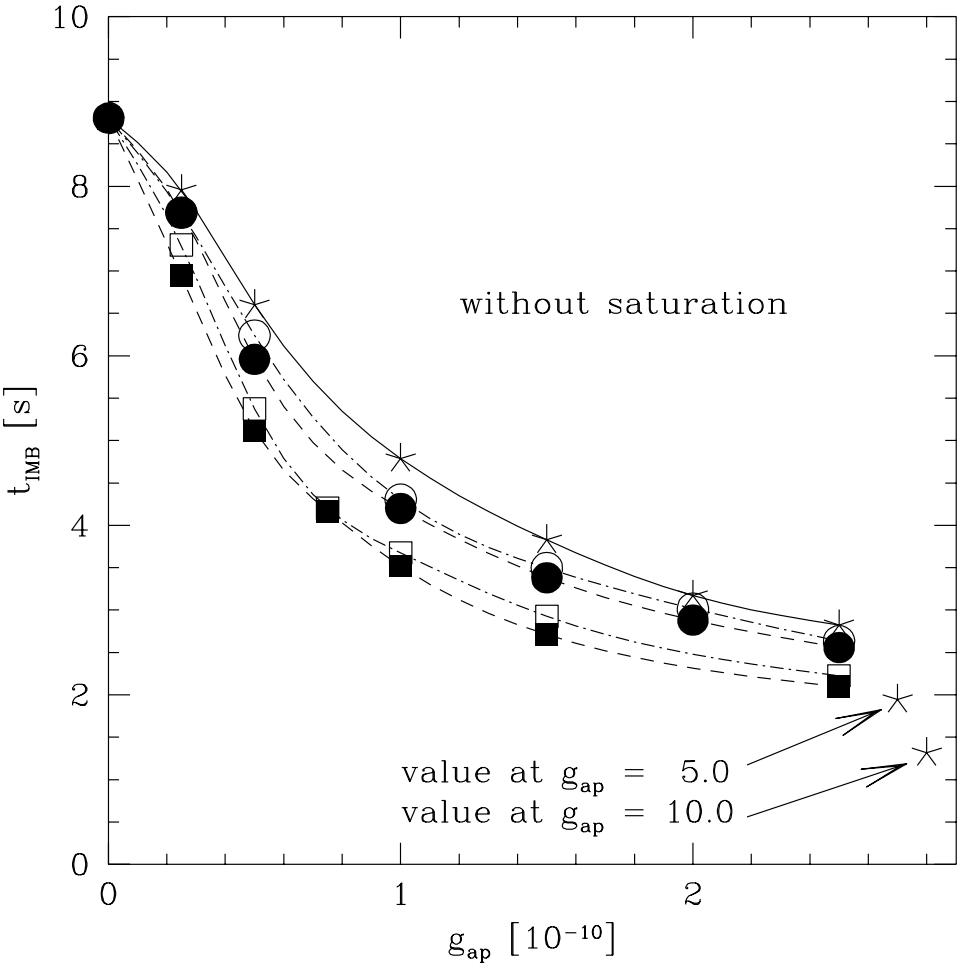


FIG. 10. Same as Fig. 8, but for the IMB detector.

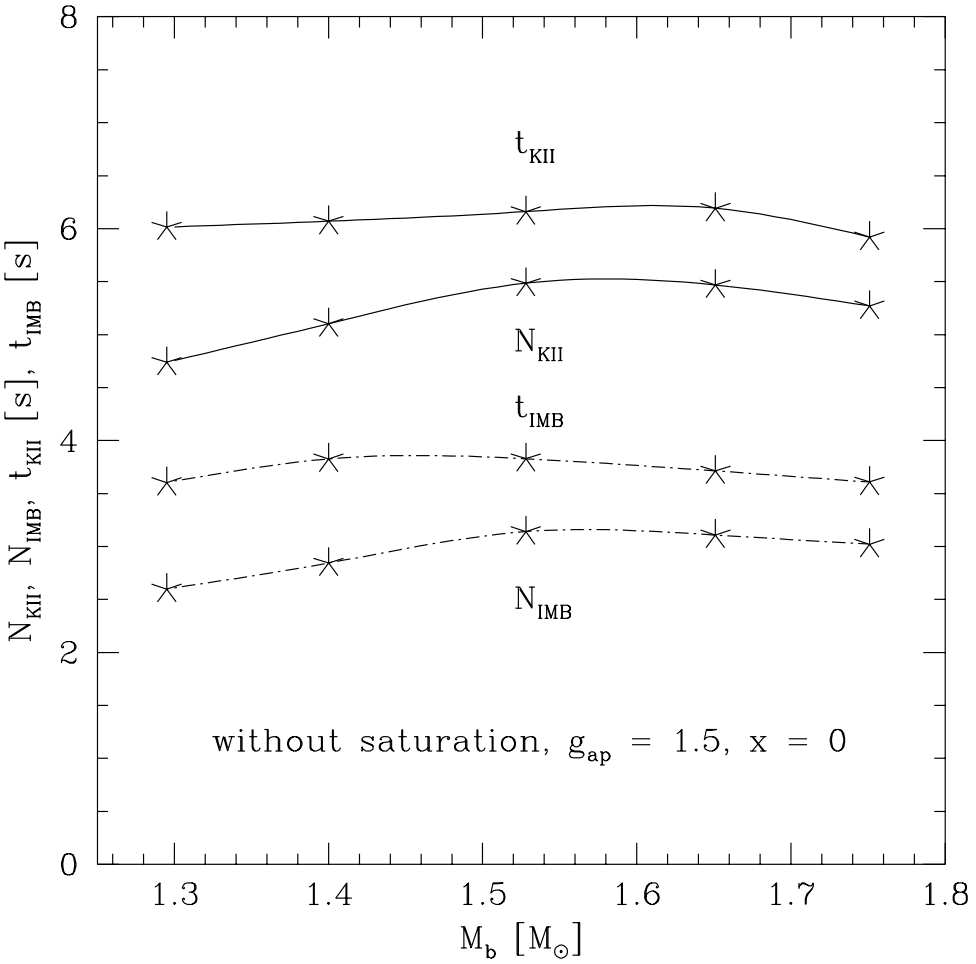


FIG. 11. Numbers of predicted $\bar{\nu}_e$ absorption events in the KII and IMB detector, $N_{\rm KII}$ and $N_{\rm IMB}$, respectively, and corresponding time intervals $t_{\rm KII}$ and $t_{\rm IMB}$ where 90% of these events happen. Five protoneutron star models with different baryonic masses, $M_{\rm ns,b} = 1.30\,M_\odot$, $1.40\,M_\odot$, $1.53\,M_\odot$, $1.65\,M_\odot$, and $1.75\,M_\odot$ were evolved with axion emission by nucleon-nucleon bremsstrahlung [Eq. (12)] for $g_{ap} = 1.5 \times 10^{-10}$ and $x = g_{an}/g_{ap} = 0$. The expected measurements for event numbers and detection times vary extremely weakly with $M_{\rm ns,b}$.

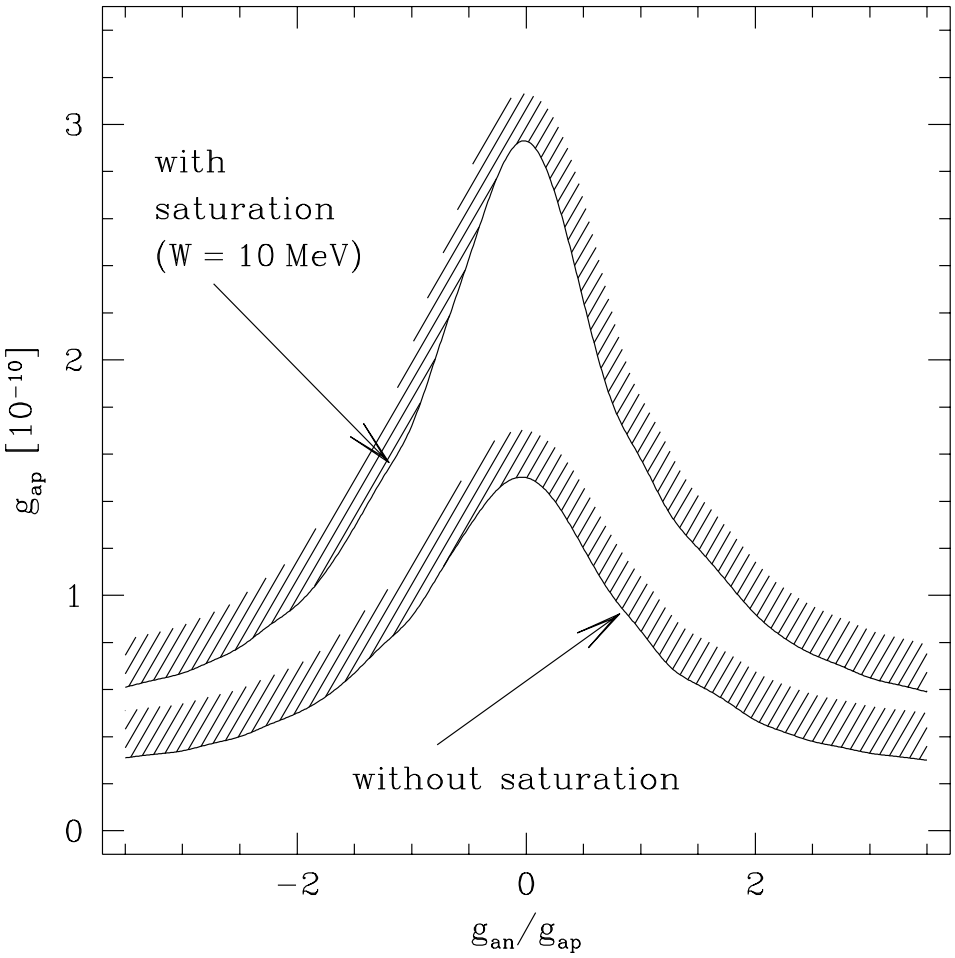


FIG. 12. SN 1987A limit to the axion proton coupling as a function of the ratio of the axion-neutron to axion-proton couplings, with and without saturation due to many-body effects. Saturation (for an average interaction energy per nucleon of $W = 10\,\mathrm{MeV}$) degrades the limit by a factor of about 1.9 independent of the ratio of the axion-neutron to axion proton couplings. The combinations of coupling parameter values above the bell-shaped curves are excluded.

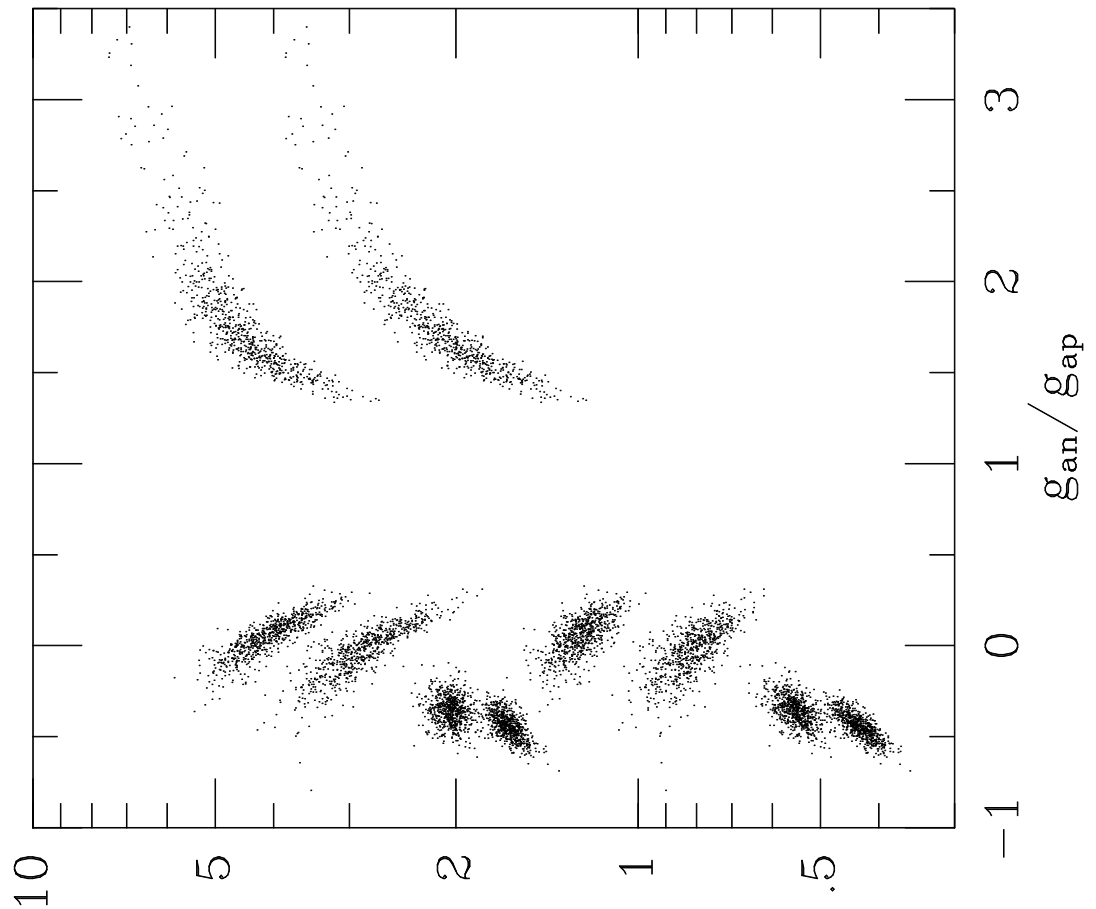


FIG. 13. SN 1987A limit to the axion mass as a function of the ratio of axion-neutron to axion-proton couplings for different axion models, with (lower set) and without (upper set) pion processes; from bottom left to top right, $\beta = 0$, $\beta = 27°$, KSVZ, $\beta = 54°$ and $\beta = 81°$. Note that saturation due to many-body effects has not been included (it degrades the limit by a factor of about 1.9).